An Evaluation of Observing Constellation Orbit Stability, Low Signal-to-Noise, and the Too-Short-Arc Challenges in the Cislunar Domain

Mark Bolden, Timothy Craychee, Erin Griggs
Trusted Space, Inc.

1. ABSTRACT

When designing an effective architecture for Space Domain Awareness (SDA) it is necessary to perform extensive modelling across multiple disciplines to effectively design network distributions, sensing payloads, concepts of operations (CONOPs), and Orbit Determination (OD) algorithms. To produce timely domain awareness requires sufficient coverage from well calibrated sensors with real-time data reduction, orbit generation, object characterization, event alerting, and dissemination. The cislunar domain introduces new SDA challenges, such as larger volumes to monitor, lower signal to noise ratios, line of sight obstruction from the Moon, on-board processing/orbit generation to maintain timeliness, lack of GPS for position, navigation, and timing (PNT), limited observatory size weight and power (SWaP), limited communication availability, three body orbit instabilities, and a vast diversity of potential orbit trajectories due to the lunar gravitational forces. Architecting solutions that address these complex challenges requires significant modeling and simulation from diverse areas of expertise to ensure all major contingencies are well represented. This paper will discuss three major challenges for performing cislunar domain awareness: low Signal-to-Noise Ratios (SNRs), Too-Short-Arcs (TSAs), and Observing Constellation Orbit Stability (OCOS).

2. INTRODUCTION

Though Earth orbiting domains have offered strategic military value since the first satellite was launched into the space domain, the cislunar domain, in contrast, has been a domain of exploration. While traditional space faring nations, such as the United States (US), China, Russia, and Europe, have leveraged the Earth orbiting domain for military functions for decades, other nations are entering the space domain as well. For example, India recently tested an anti-satellite weapon [1] and Iran just launched their first satellite into low Earth orbit (LEO) [2]. Meanwhile, Russia, Japan, China, and the US have recently released plans to return to the Moon [3] [4] [5]. China has placed a communications satellite at the L2 Lagrange point and recently reported the first successful rover mission to the far side of the Moon [6] [7]. While the cislunar domain does not hold inherent military value, it provides adversaries a new way to "hide in space." Objects in cislunar space are extremely difficult to track with current capabilities. Low SNR due to vast distances and lunar exclusion zones prevent existing space tracking systems from providing custody of cislunar objects. Orbits such as the free return trajectories developed for the US Apollo missions, can be repurposed very easily to both mask the origin of a spacecraft, and to potentially re-enter the Earth orbiting domain with no concern for attribution.

Multiple sources agree that deterrence is the best approach to ensuring the cislunar domain is not leveraged for nefarious purposes. This requires an uncooperative tracking architecture that enables attribution of spacecraft to the owner operator from launch to spacecraft end-of-life. The 4π steradian cislunar domain that extends out to the L2 position encompasses a volume of 3.79×10^{17} km^3. This volume dwarfs the typically discussed SDA volume that extends out to the geosynchronous belt, only 3.14×10^{14} km^3. With volumes of this size, the ranges from observer to object are substantial with a maximum potential range of 898,200 km. This introduces two key challenges: low SNRs due to range and TSAs due to slow apparent angular motion. For active systems, SNR drops proportionately to 1/range^4, and for passive systems, by 1/range^2. For example, a diffuse sphere in geosynchronous orbit with an albedo of 0.17 and a surface area of 1 meter^2 is >15 visual magnitudes when viewed from the Earth's surface, whereas at maximum distance in the cislunar domain for the same object size is >22 visual magnitudes. The increased range also effects the observed arclength when viewing an object from another distant object. This presents a significant challenge when performing Initial Orbit Determination (IOD) due to poor sampling of the new object's in-track velocity. This is a well-known problem when observing geosynchronous objects from the Earth's surface and is commonly referred to as the Too Short Arc (TSA) problem. These two challenges push the trade space for cislunar SDA to consider space-based platforms that are distributed throughout the cislunar domain to reduce ranges from observer to target, introduce illumination diversity, and astrometric diversity. However,

expanding the trade space to include cislunar orbits introduces significant challenges for Observing Constellation Orbit Stability (OCOS) due to the three-body Earth-Moon-observer challenge.

The cislunar orbit trade space for the three-body Earth-Moon-observer is complex. This is due to the gravitational forces applied to the observer's orbit within the cislunar volume, specifically, the relationship between the observer's location and the Moon. The Moon's gravity has the potential to make observer's orbit chaotic in nature to include high swings in orbital parameters, specifically inclination, apogee, and perigee values. In some cases, if not properly monitored and controlled, the lunar gravity can create an Earth reentry scenario. The Moon's gravity also has the potential to induce orbit stability as well. The best example of these locations are the Lagrange points, specifically, the L4 and L5 points which are extremely stable. Additionally, there are multiple families of periodic orbits including Halo orbits around a Lagrange point. The three-body problem induces complexities when performing initial orbit determination, by requiring multiple factors to be considered (e.g. Earth Centric System, Moon Centric System) and the timelines involved. Without diverse geometric collection, the information gained between observations is limited resulting in extremely large uncertainties.

This paper will discuss a process for modeling and simulating the cislunar domain to evaluate concepts for Cislunar Space Domain Awareness (SDA) network architectures with specific architecture examples. Specific challenges to be discussed include low Signal-to-Noise Ratios (SNRs), Too-Short-Arcs (TSAs), and Observing Constellation Orbit Stability (OCOS). Example cislunar SDA network architecture simulations will be discussed for attempting to detect and obtain custody of an object on a lunar free-return trajectory. A comparison of the effectiveness for each architecture design will be discussed with common metrics of performance.

To visualize orbits in this paper, we leveraged the General Mission Analysis Tool (GMAT), a Free and Open Source Software (FOSS), to model and simulate the various orbits and constellations under evaluation. GMAT provided the capability to perform full force modeling of orbits around various central bodies (e.g. the Earth or the Moon). GMAT's full force model enables factors such as atmospheric drag, solar radiation pressure, gravity models both high fidelity (e.g. WGS84 for the Earth) and point mass (e.g. Sun, Moon), and other factors to be considered when propagating an orbit. The incorporation of the full force model allows propagation results to be trusted because the simulated environment will match that of the actual environment. By not leveraging a full force model, a solution may be obtained that while it looks like it will address a problem, it in fact breaks down and is invalid in the actual space environment.

For the purposes of this research, Systems Tool Kit (STK) provided the capability to analyze multiple spacecraft simultaneously. Additionally, the ability to analyze data in multiple reference frames and its ability to generate data quickly without having to propagate for each run saved significant time and effort. STK's suite of internal data providers enabled data to be populated in both report and graphical form based on the information need. This included looking at data in the form of classical orbital elements, the position of the Sun with respect to the spacecraft, or other information.

To assist in understanding the outcome of an orbit simulation, we leveraged two different reference frames: Earth J2000 (Figure 1) and Earth-Moon Rotating (Figure 2). The Earth J2000 is the typical standard reference frame when propagating and visualizing an orbit. The reference frame is a function of the Earth's orbital plane and the Earth's rotational axis. As the Earth rotates, the J2000 frame will stay near stationary, as the Moon rotates around the frame. The relevance of this frame is it enables a view to understand the relationship of an orbit with respect to the Sun as the orbit will rotate with the Sun. This can be seen in Figure 1. The Theta (Θ) value in the figure remains constant as celestial bodies move with respect to one another.

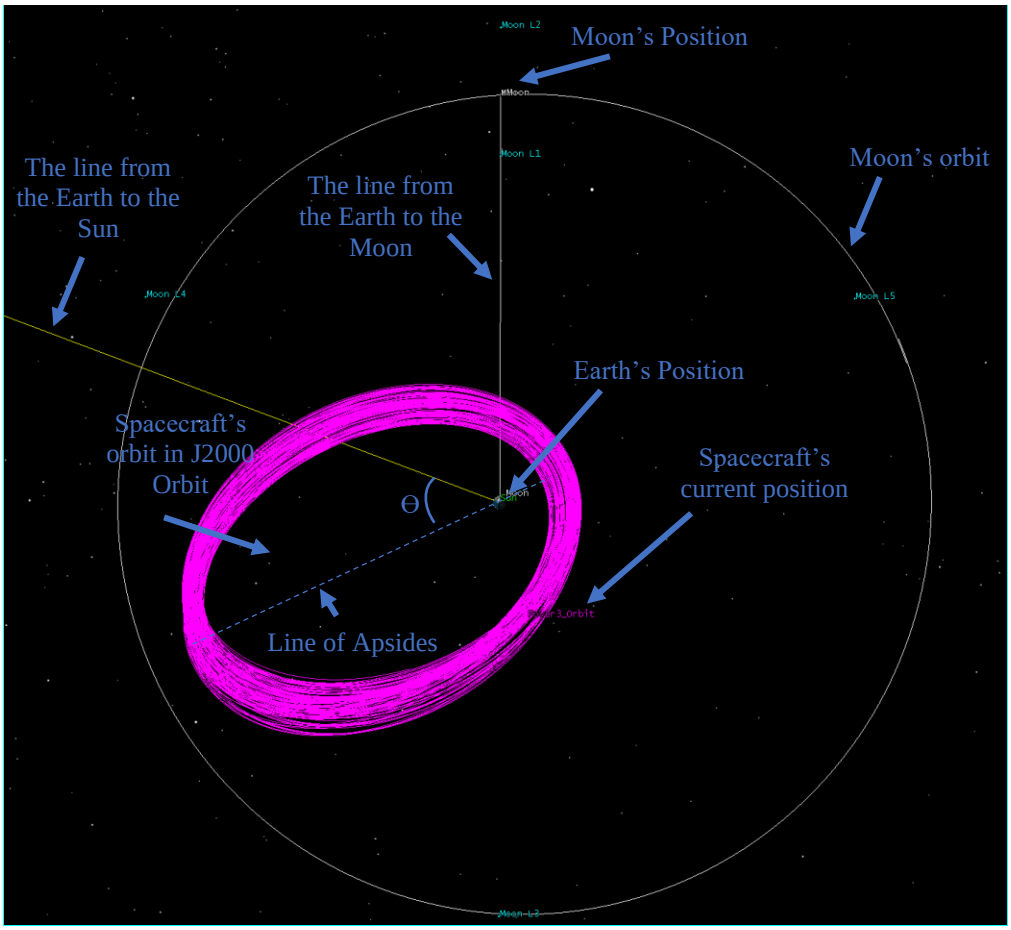

Figure 1: J2000 Reference Frame

The Earth-Moon Rotation frame, Figure 2, can be considered a "fixed-like" frame not to be confused with the Earth Fixed frame. In the Earth-Moon Rotating frame, the location of the Earth and the Moon are essentially fixed (the Moon's location moves slightly over time due to is non-circular orbit). This frame also is important when showing the Earth-Moon Lagrange points as they are also essentially fixed in space. When visualizing an orbit simulation, as in Figure 2, the spacecraft's orbit is shown with respect to this frame and the relationship of the spacecraft's orbit with respect to both the Earth and Moon is clearly visible. It is important to note that the Sun's position rotates around this frame over a ~29-day period.

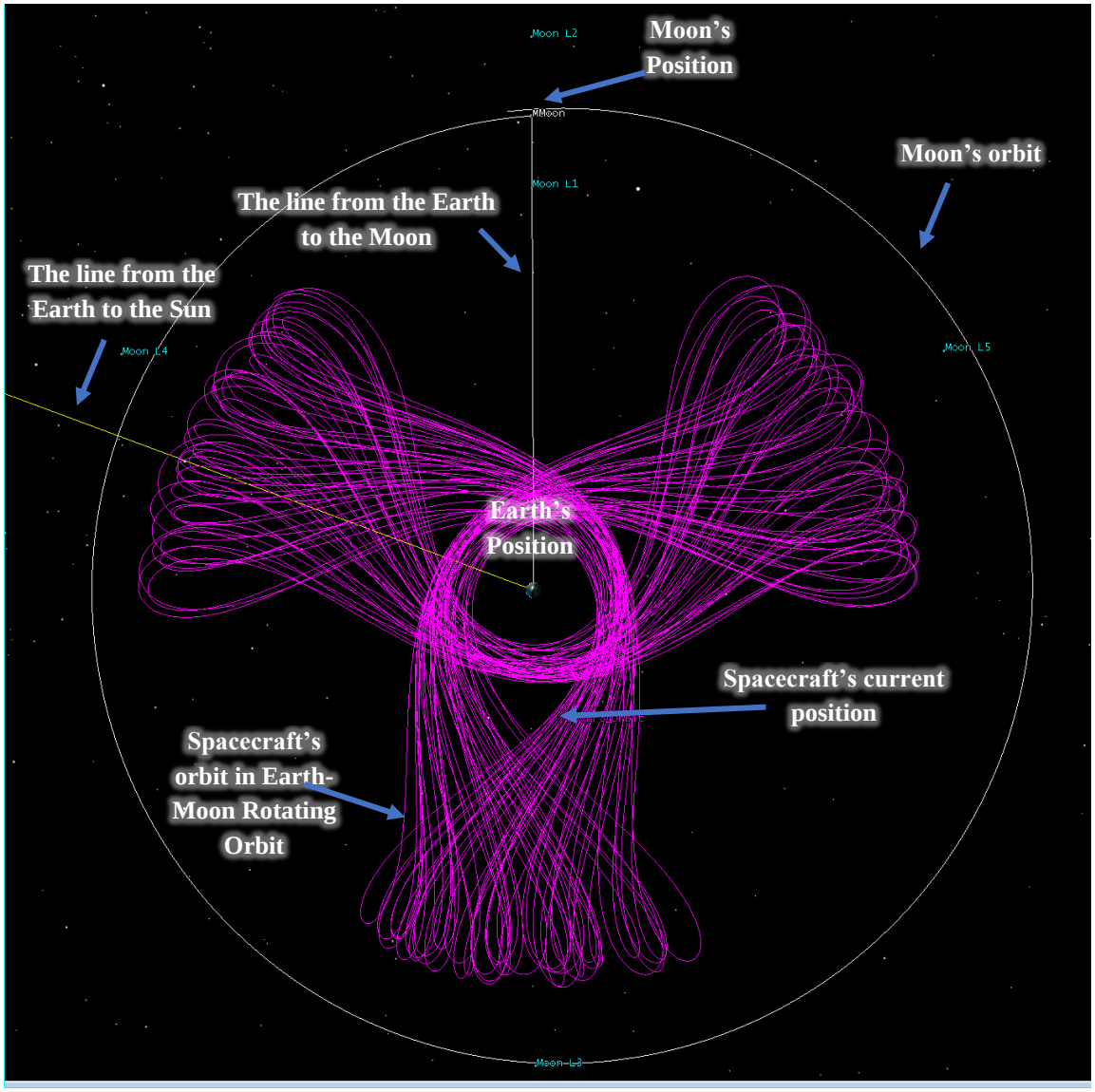

Figure 2: Earth Moon Rotating Reference Frame

Lastly, it is important to note that Figure 1 and Figure 2 are showing the exact same information in different reference frames.

3. POTENTIAL CISLUNAR TRAJECTORIES

Full cislunar domain awareness requires observing and detecting objects that are operating within the 4π steradian volume. This volume has an inner radius starting approximately at 42,000 km (Earth Geostationary Orbital Distance) and an outer radius of approximately 475,000 km (Distance from the Earth to the 30,000 km beyond L2). This volume is significant, approximately 449 quadrillion km^3, and provides ample opportunity for spacecraft to hide and operate in plain sight without being detected. The following section describes the collection of orbits and ballistic trajectories that spacecraft have operated in or have been theorized to operate in.

Spacecraft operating in this environment may transition between one or more of these types depending on the current operations of the spacecraft adding complexity when tracking and maintaining custody of these objects. This may require multiple hypothesis to be used to appropriately track and predict when and where a spacecraft is

going to be. Additionally, the environment will play an important role as the gravitational forces exposed to the spacecraft may transition as well. This may include changes from an Earth centered focus to a Moon centered focus and/or a combination of the Earth, Moon, and Sun. This is especially relevant for those objects that are traveling near or to the Moon and the L1, L2, L4, or L5 Lagrange points located in the vicinity in the Moon and shown in Figure 3.

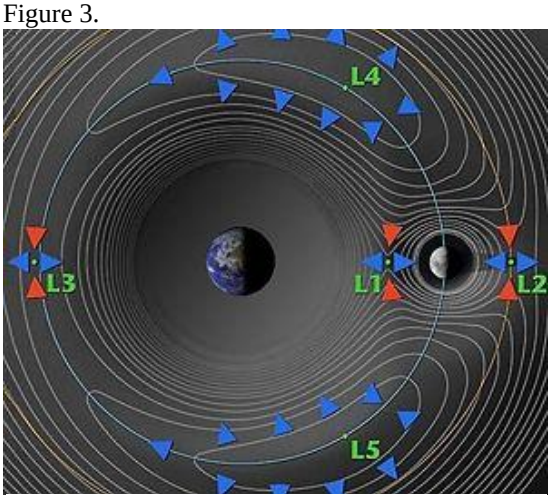

Figure 3: Cislunar Domain with Earth-Moon System Lagrange Points [23]

Spacecraft operating in the Earth-Centered cislunar space with an orbital period that is not resonant with Moon's orbit are typically unstable and referred to as chaotic systems. These orbits are typically highly eccentric, and their chaotic nature is due to the impact of the lunar gravity. The Moon's force can change the apogee and perigee of the orbit but also impacts the inclination of the orbit as well. This creates wild oscillations and, if not maintained, the orbits potentially have ability to intersect with the Earth. An example of this orbit type is the early operations of the NASA IBEX spacecraft.

The highly inclined orbit is a special case of the chaotic system. In this case a lunar swing-by is typically used to significantly change the inclination of the spacecraft's orbit. Once the lunar swing-by occurs the satellite is left in an Earth orbit to perform its mission. The NASA Lunar Crater Observation and Sensing Satellite (LCROSS) mission is an example of this orbit type.

The opposite of chaotic systems, orbits with a period that is resonant with the Moon (1:2 (Moon: Satellite) or 1:3) have been identified as very stable. These orbits do not require significant propulsion to maintain their trajectories. These orbits are now being utilized by research agencies due to their low-cost during satellite operations. Example missions include NASA IBEX and TESS.

Phasing loops are a strategy developed to reduce the overall cost of launch and inserting the spacecraft into a cislunar or lunar orbit. Instead of utilizing a direct transit maneuver, the spacecraft performs multiple orbits around the Earth and at perigee a maneuver is performed to increase apogee. Typically, one of two actions occur once apogee reaches the intended altitude: 1) The spacecraft reaches the mission apogee altitude and then performs one or more burns at apogee to increase perigee altitude resulting in final Earth orbit, or 2) The spacecraft has an altitude where the lunar gravity takes ahold of the spacecraft and the spacecraft performs maneuvers to enter orbit around the Moon. Each loop may enter and exit the 4π steradian volume depending on the perigee altitude. Phasing loops present two challenges: 1) They do not require large launch vehicles to enter the 4π steradian volume, and 2) The orbits rotate with the Earth-Moon rotating frame which adds complexity from a tracking perspective. These challenges are beneficial from the opposite viewpoint. Example missions include NASA IBEX and Lunar Atmosphere and Dust Environment Explorer (LADEE).

The free return trajectory is the typical cislunar orbit from the NASA Apollo missions. Unlike the phasing loops, this is a direct transfer from either launch or low Earth orbit (LEO) between the Earth and the Moon. These orbits are typically days (Earth to Moon and back) whereas phasing loops may be a month or more in duration. The free return trajectory is also dependent on utilizing the Earth and Moon's gravity model at different points during the orbit. As a result, this is an Earth and Moon centric orbit.

Like phasing loops, operators of spacecraft intended to be delivered to a Geostationary (GEO) orbit have leveraged a lunar swing-by to insert the spacecraft into GEO. This is not a nominal operation and usually occurs when the spacecraft is (typically "stuck") in a Geostationary Transfer Orbit (GTO). A GTO orbit to GEO addresses two factors: 1) It sets the apogee and perigee to GEO altitudes, and 2) It changes the inclination based on the launch location to that of a GEO orbit. The lunar swing-by changes the inclination of the vehicle, typically a costly maneuver. However, recent publications show that this method could be utilized to launch spacecraft where the launch location has high latitudes. An example use of this orbit type is AsiaSat3, now called PAS-22.

Lunar transit is likely a subset of other types listed in this document. Additionally, the lunar transit can be used to capture objects from various points (Lagrange points, Heliocentric orbits, etc.) and have them enter the 4π steradian volume. Using a lunar swing-by, sometimes multiple, is beneficial in many ways, especially when changing orbital parameters that are fuel expensive (e.g. inclination) or using the lunar gravity with the appropriate maneuvers to speed up or slow down spacecraft to hit their intended targets. The lunar transit can be considered a waypoint in a spacecraft's trajectory. At this waypoint spacecraft can either enter or exit the Earth/Moon system altogether or be used to change the spacecraft's primary orbiting central body (e.g. Earth to Moon or Moon to Earth). Example missions include International Sun-Earth Explorer 3 (ISEE-3), LADEE, Lunar Reconnaissance Orbiter (LRO), and TESS.

A special case of lunar transit is the ballistic lunar capture transfers also known as Weak Stability Boundary (WSB) transfers. WSB transfers leverage the chaotic dynamics around the Moon to enable the capture of a spacecraft launched directly from the Earth into lunar orbit and are highly efficient from a fuel usage perspective. An example mission is the Hiten satellite.

With every large planetary body system (Earth/Moon, Earth/Sun, etc.) the locations where gravitational forces cancel between the central bodies are known as the Lagrange points. As stated above for each system there are five points. The L1, L2, and L3 points are unstable, requiring maneuvers to maintain an orbit around the point. The L4 and L5 points are stable and are wells in the gravity profile where objects can collect naturally.

In multibody systems, there are various families of periodic orbits. These families can be identified by looking at the primary central bodies (e.g. Earth and Moon) and their respective mass ratio. In the Earth-Moon system the mass ratio is mu = M2/(M1 + M2) = 0.01215. It is this mass ratio that leads to the Lagrange points which are a specific family of three-body orbits. Additionally, there are a series of orbits that emanate and orbit around the Lagrange points. These can be Planar (in the same plane as the Earth and Moon), Axial (intersect the x axis at two points), and Vertical (emanate from L# points).

The very high-altitude ballistic trajectory addresses those objects that launch from the Earth and return to the Earth but never reach orbital velocities. In theory, these could also cover launches from the Moon if an event were ever to occur. For the Earth specific example, the high-altitude ballistic trajectory has apogees that are beyond the GEO orbit. The intent of these trajectories would be hostile in nature.

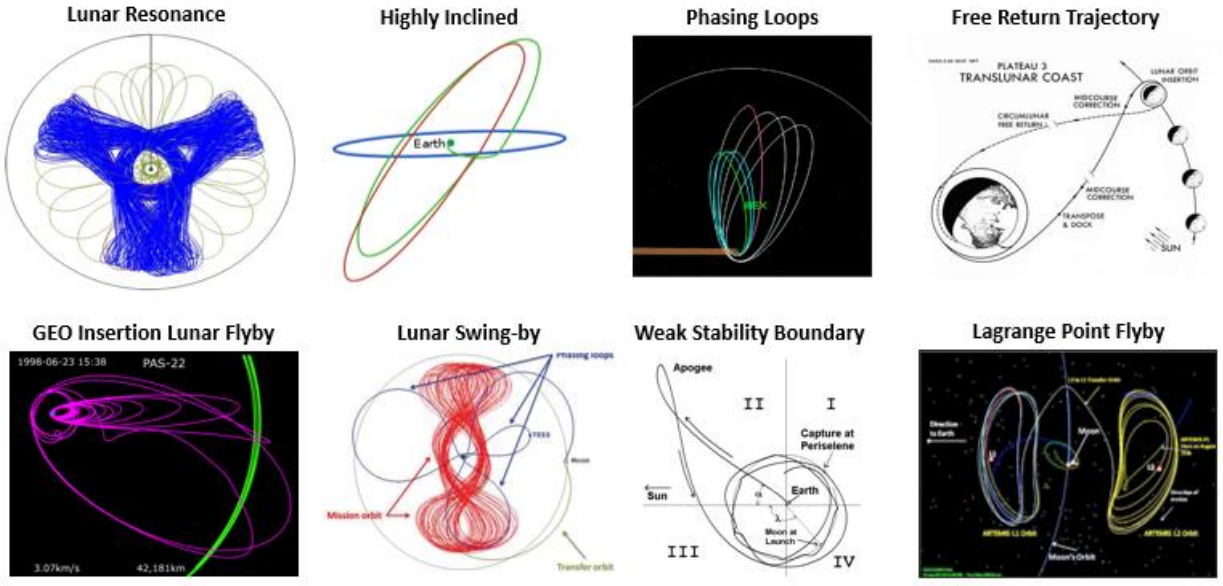

Figure 4: Cislunar Trajectory Types [8] [9] [10] [11] [12] [13] [14] [15]

4. SIGNAL TO NOISE RATIO CHALLENGES

When designing a tracking system, the most important consideration is the system's ability to detect the objects of interest. This is analyzed by modeling the system parameters, CONOPs, and the object of interest to determine if there is sufficient signal for detection, typically quantified as the signal to noise ratio (SNR). A wide variety of publications are available discussing SNR as applied to optical Charge Coupled Device (CCD) detections [16]. Due to the vast distances encompassed by the 4π steradian cislunar volume and the large diversity of potential solar phase angles, achieving sufficient SNR poses a significant challenge. The sensor design, sensing platform stability, location, CONOPs, and target parameters contribute to the SNR. Simulations must account for as many of these parameters as possible to estimate the expected performance. For example, the CONOPs directly affects the SNR by determining how much the object signal is distributed across the focal plane.

For this study, we modeled different CONOPs and constellations to evaluate different architecture designs based on consistent metrics. These results were leveraged to compare the performance of full architectures for un-cued search of the entire domain and cued rate tracking for custody of specific trajectories. The constellations and candidate trajectories simulated were leveraged as inputs to a dynamic signal to noise ratio (SNR) analysis to determine domain volume coverage, revisit rates, and object custody in the cislunar domain.

Fundamentally, the simulations were performed to answer two questions as a function of the domain and object positions over time:

1. Does the payload have line of sight (LOS) to the object location / domain region?
2. Does the payload have sufficient SNR to detect the object class?

The answer to the first question was determined by modeling the orbit geometries with a specific payload/bus/constellation CONOPs against specific targets and a three-dimensional grid that represents the domain location in the respective coordinate frame. In addition, geometric logic statements determined two criteria:

1. Is the object location / domain region within the field of view?
2. Does the object location / domain region fall within any exclusion zones?

If the geometries provide LOS to view the object, a check for sufficient SNR is performed by modeling the object state vector, object size/albedo, observer state vector, domain region state vector, payload, CONOPs, and illumination conditions. The simulation produced two result types that can be leveraged to generate additional metrics:

1. Time stamped SNRs for each line of sight from observers to the object.
    - Provides the data necessary for producing additional metrics such as time from launch to detection, number of detections per hour, etc. for a specific orbit/object class.
2. A three-dimensional histogram of the number of revisits with sufficient SNR to detect the object class.
    - Provides the data necessary to identify potential gaps in the overall domain coverage.

As different constellations were evaluated in this process, the results were fed back into the overall constellation design to adjust orbit type(s), constellation size(s), etc. We made significant progress in evaluating various cislunar observer mission profiles through extensive modeling of trajectory profiles and potential architectures. The benefits, weaknesses, and gaps associated were identified for each evaluated architecture. As new results were generated, each architecture was adjusted to better meet the mission objectives. This included altering orbital parameters, constellation sizes, orbit type(s)/combinations, and CONOPs. For each architecture, the mission profile was assessed for overall un-cued domain coverage and custody effectiveness for specific object trajectories, both cued and un-cued. In addition, potential challenges specific to each architecture were evaluated. The overall mission profile effectiveness of each potential architecture for cislunar domain awareness was evaluated through two key analyses:

1. Domain Coverage & Gap Analysis
2. Object Custody Analysis

The first analysis was performed on each potential constellation, payload, and CONOPs to assess the number of revisits as a function of the domain to identify regions where there is sufficient coverage and regions where there are gaps. These results are presented in the form of interactive three-dimensional renderings, and a two-dimensional plot comparing revisit counts as a function of percentage of the domain. The goal of the three-dimensional

renderings is to understand the strengths and weaknesses of a simulated architecture quickly and intuitively. The following narrative with figures will detail how these renderings are to be interpreted.

First, the domain was defined. For this use case, the domain is defined as the 4π steradian sphere that encompasses all five Earth-Moon System Lagrange points. See Figure 5.

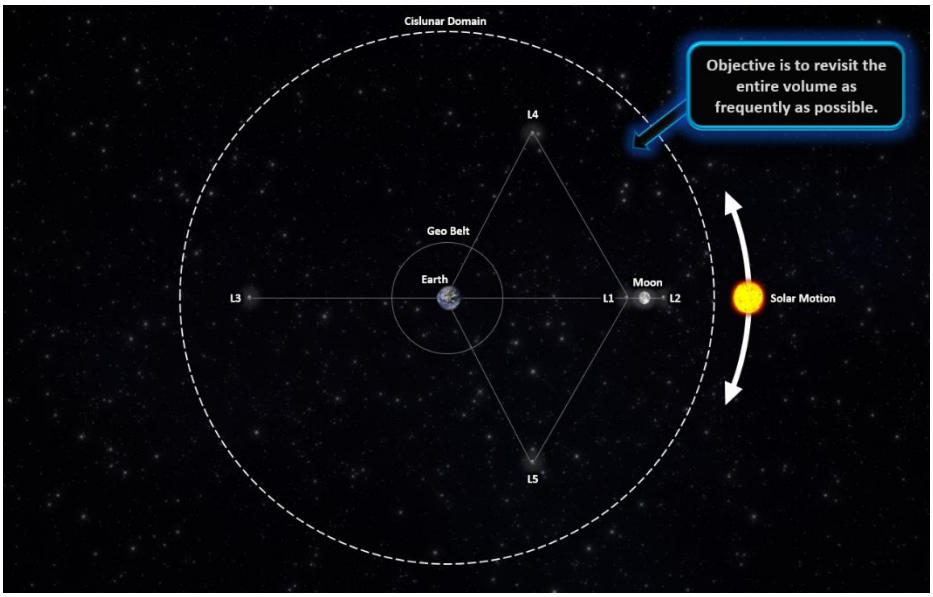

Figure 5: Cartoon Representation of the Cislunar Domain

The dashed white circle depicts the boundary surround the volume of space that must be monitored. Next, a constellation of orbits is designed to survey the full domain. This is illustrated in Figure 6 in the Earth-Moon Body Barycentric Reference (BBR) Frame.

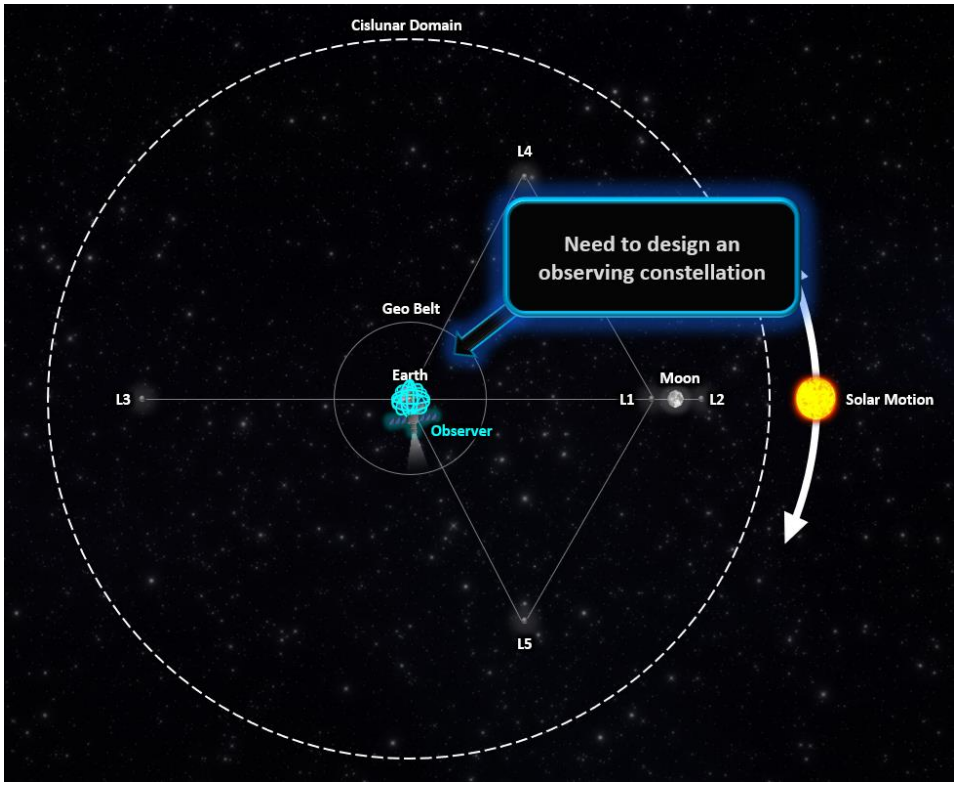

Figure 6: Cartoon of Observing Constellation in BBR Frame

An ideal constellation would revisit the entire domain, multiple times throughout the simulation. This is illustrated in Figure 7 as a histogram where high revisit counts are depicted by the color yellow.

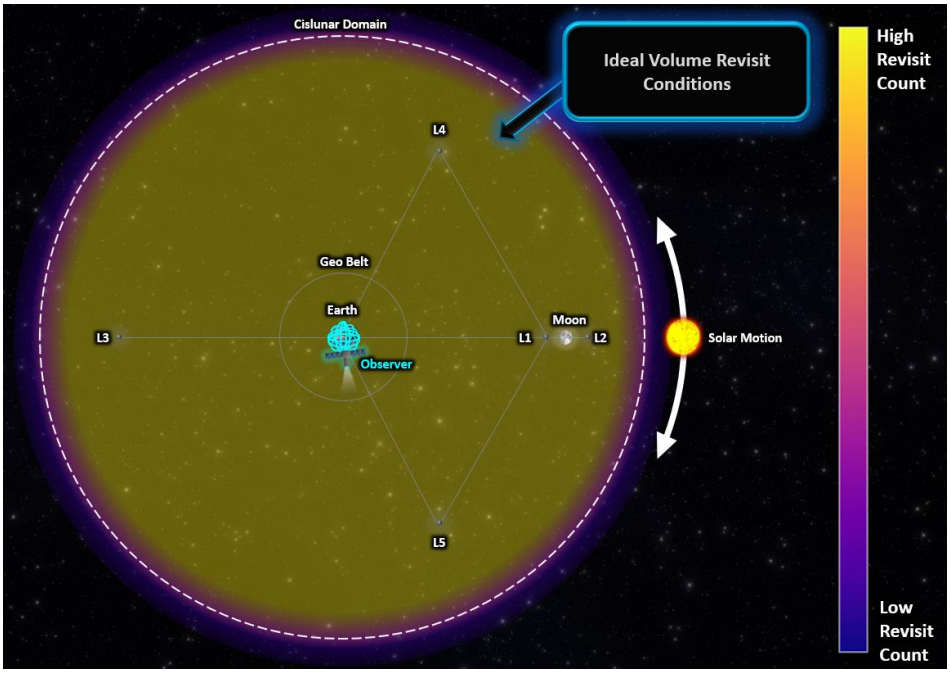

Figure 7: Illustration of Revisit Histogram for Coverage Analysis

Unfortunately, due to the challenging nature of achieving full coverage of the 4π steradian cislunar domain, most architectures are not capable of producing these types of results. One such architecture is illustrated in Figure 8. This

figure depicts a constellation that does not possess the geometric diversity necessary to detect small objects with low solar phase angle. As a result, over half of the domain represents a gap in coverage.

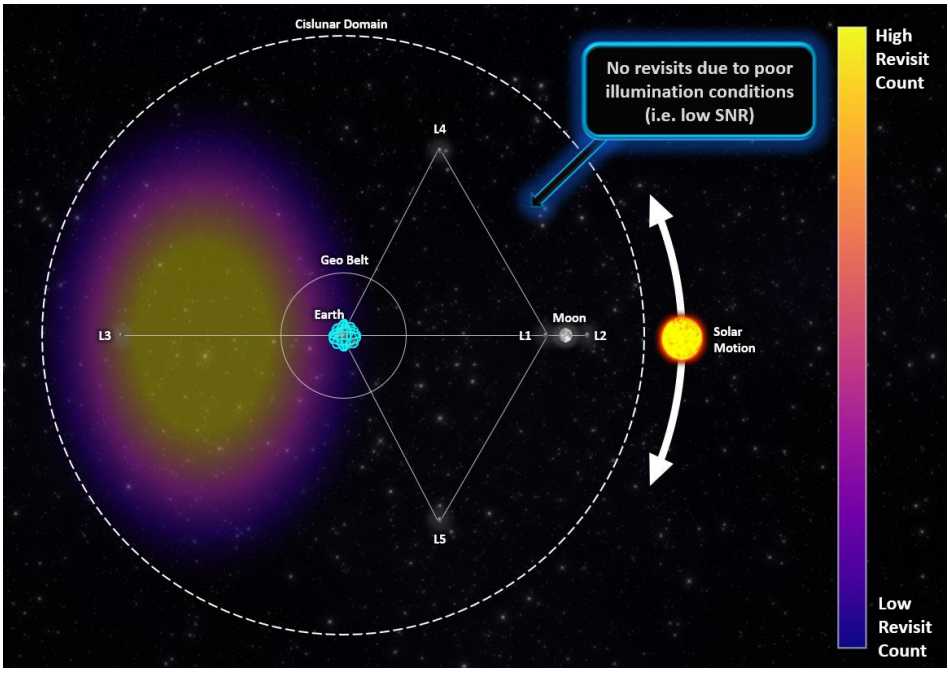

Figure 8: Illustration of Architecture with Insufficient Coverage

In addition, it was helpful to understand which gaps are due to poor SNR and which are due to exclusion zones, such as solar exclusion. To identify these regions quickly and intuitively, there is an additional histogram illustrated to highlight regions within the gaps that result from exclusion zones. The case of solar exclusion is illustrated in Figure 9.

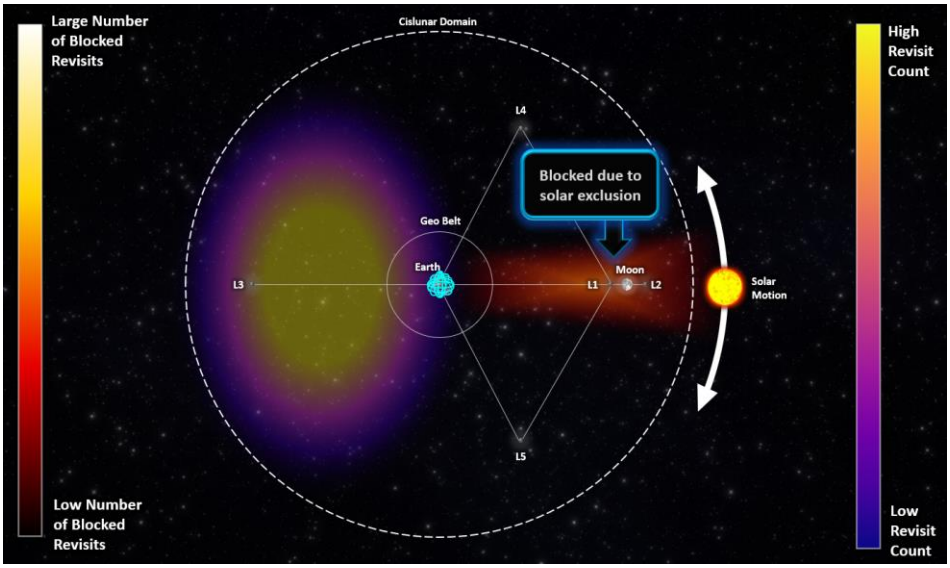

Figure 9: Illustration of Gaps due to Solar Exclusion

Through the architecture design process, we leveraged this type of analysis to rapidly compare constellations, payloads, and CONOPs to develop a solution before assuming specific object trajectories. It also provided a means to quantify the performance of different architectures purely based on the domain definition. This is shown in Figure 10 by plotting the percent coverage of the domain as a function of number of revisits in a 24-hour period.

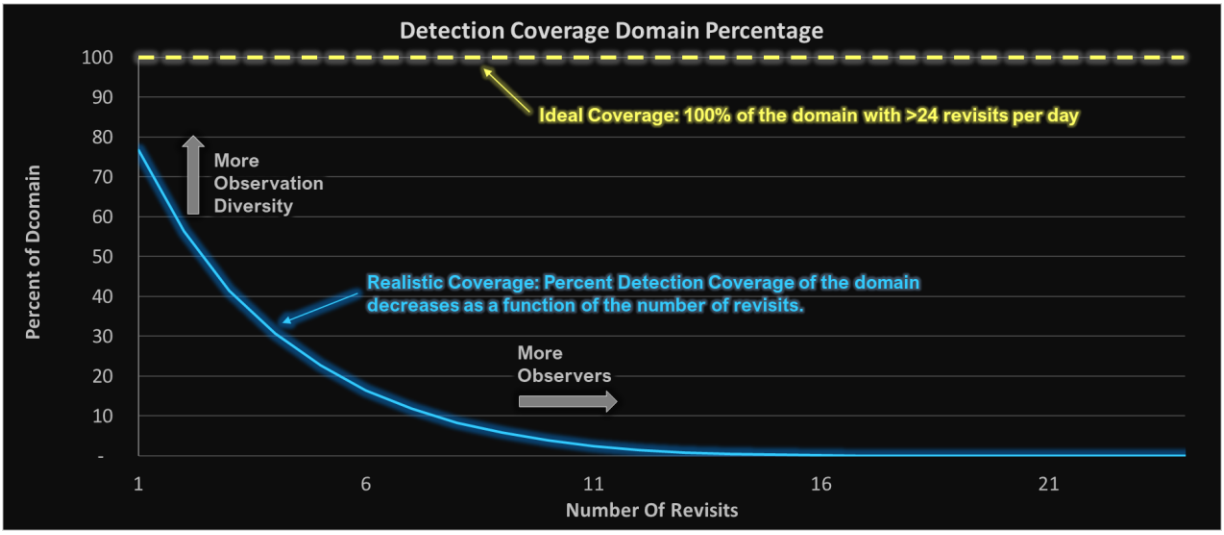

Figure 10: Detection Coverage Domain Percentage of Multiple Architectures

Figure 10 depicts two separate cases for Detection Coverage Domain Percentage. The ideal case for coverage is shown by the yellow dashed line. It represents an ideal volume coverage as depicted in Figure 7. In contrast, Figure 10 also shows a more realistic view of domain coverage in blue. This curve intuitively demonstrates an architecture with decreasing revisit rates as a function of the size of the domain. This can be improved by either creating an architecture with more observation diversity, and/or an architecture with more observers. Observation diversity can be increased by adding more diversity in geometry between observer, illumination source, and the domain volume. The observation diversity creates diversity in SNR as a function of solar phase angle and object to target range. More observers in similar geometries will increase the revisit counts for regions already observed.

Object custody was analyzed by evaluating the architecture against a specific object in both cued and un-cued CONOPs. This enables an assessment of time from launch to detection and custody persistence. Similar to the domain coverage analysis, this analysis is performed by modeling the architecture as illustrated in Figure 6, and then adding the object trajectory as shown in Figure 11.

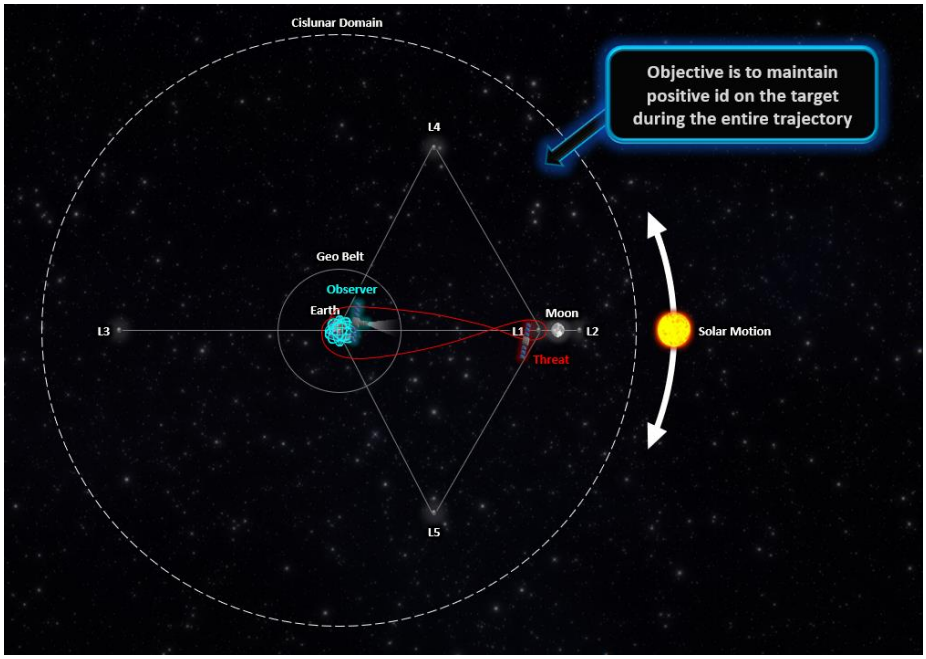

Figure 11: Illustration of Object of Interest in Domain

In this illustration a free lunar return trajectory is depicted with a constellation of observers in LEO orbit. As the object moves through the field of view the observers are each modeled with a prescribed CONOPs to determine if they have LOS and sufficient SNR to the target. When both these conditions are met, a line from observer to the object of interest is rendered to indicate custody. The SNR is used to color the line to quickly identify which geometries are providing superior SNR as shown in Figure 12.

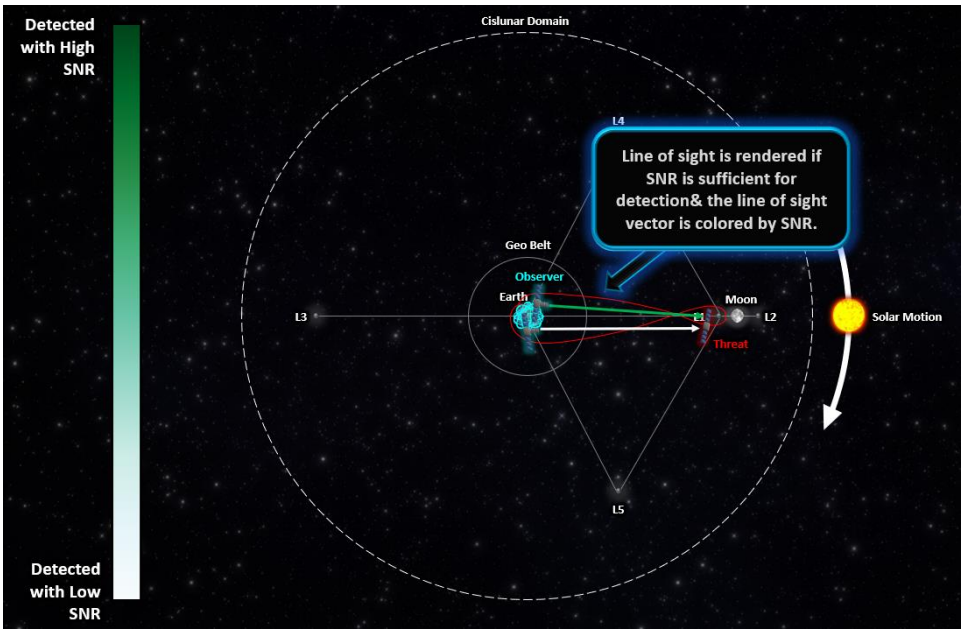

Figure 12: LOS and SNR Illustration from Observers to Object of Interest

These simulations are then also viewed more simplistically as SNR vs. Time to determine at which point in the trajectory the object is detected and when the object is undetectable during cued tracking. Figure 13 shows an example output from the simulation for the free lunar return trajectory during Full Moon against the GEO and Lagrange constellation while performing cued tracking of the object. The required SNR for detection is also plotted. In this example it is apparent that some of the observers can successfully detect the object however there are also significant gaps in coverage due to low SNR. Only the detections in green in Figure 13 will be rendered as detection vectors in Figure 12.

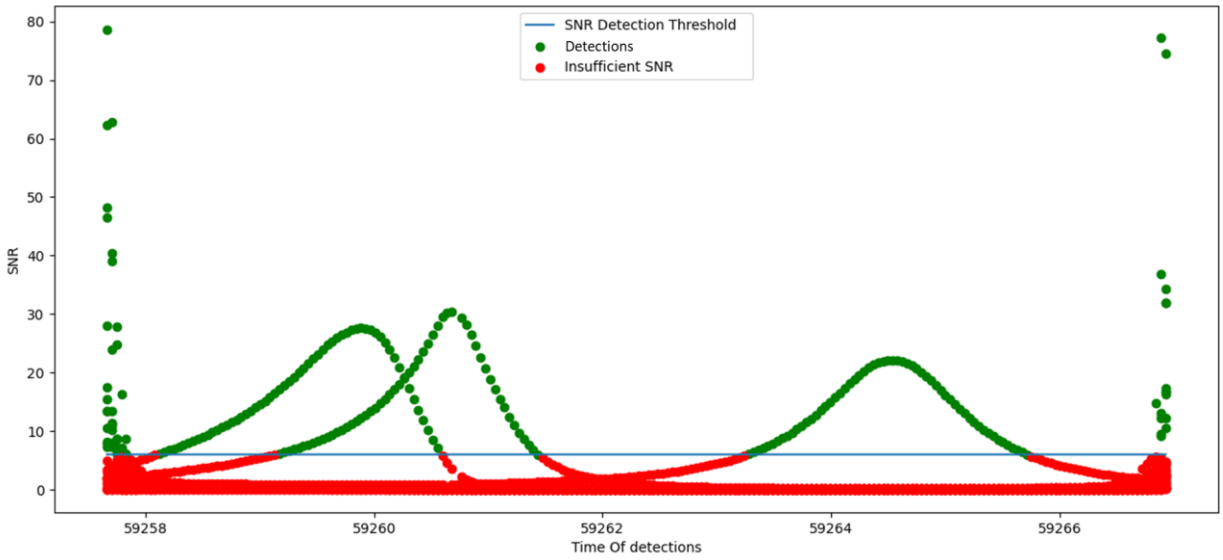

Figure 13: Example Cued Custody Plot for Waxing Crescent Free Return Trajectory

Cislunar Domain Awareness Mission Analysis

We analyzed a variety of domain awareness architectures for un-cued awareness and cued object custody in the cislunar domain. While many architectures were modeled and simulated, this discussion will focus on the architecture types described in Table 1 and Table 2.

In the following discussion, each architecture was modeled leveraging a 42 cm telescope with a 1.8 degrees field of view operating in the visible spectrum. A diffuse sphere with an albedo of 0.17 and a surface area of 1 meter^2 was modeled for the analysis in this paper. All CONOPs modeled assumed that the payload modeled is scanning the domain by moving from starfield to starfield and rate tracking the stars. While in some cases this causes the objects to streak across the focal plane, at longer distances the object's angular streak rate is minimal. It also provides a data type that may be image differenced by revisiting the star field, and/or jitter corrected in stacking by centroiding the stars and shifting frames before stacking. Neither of the benefits from these approaches are modeled in the following SNR analysis, however the CONOPs is designed to enable these strategies without degrading single frame processing performance. Table 1 outlines the specific CONOPs used for each orbit type. These CONOPs were designed to maximize the effectiveness of each orbit type to cover the domain and detect the objects of interest when performing un-cued search.

Table 1: CONOPs Modeled for Each Orbit Type

Constellation Architectures	Survey CONOPs Modeled
LEO Only	Initial Exposure pointing Directed in the Velocity Vector with Sidereal Tracking
GEO Only (Two Cases)	Initial Exposure pointing Directed in the Velocity Vector with Sidereal Tracking
	4π Steradian Scanning with Sidereal Tracking
Lagrange Only	4π Steradian Scanning with Sidereal Tracking
P/3 Only	4π Steradian Scanning with Sidereal Tracking
Chaotic Only	4π Steradian Scanning with Sidereal Tracking
LEO & Lagrange	Initial Exposure pointing Directed in the Velocity Vector with Sidereal Tracking
	4π Steradian Scanning with Sidereal Tracking
GEO & Lagrange	4π Steradian Scanning with Sidereal Tracking
	4π Steradian Scanning with Sidereal Tracking
GEO, Lagrange, & P/3	4π Steradian Scanning with Sidereal Tracking
	4π Steradian Scanning with Sidereal Tracking
	4π Steradian Scanning with Sidereal Tracking
P/3 & Lagrange	4π Steradian Scanning with Sidereal Tracking
	4π Steradian Scanning with Sidereal Tracking
GEO, Lagrange, & Chaotic	4π Steradian Scanning with Sidereal Tracking
	4π Steradian Scanning with Sidereal Tracking
	4π Steradian Scanning with Sidereal Tracking

Prior to developing full constellations, each orbit type under consideration was modeled over a 2-month period to determine the advantages and disadvantages of a full phased constellation of that orbit type. By running the simulations for that period, the entire orbit trajectory in the Earth Moon BBR frame is visited at least once. This provides important insight into the maximum amount of coverage possible on shorter time scales, such as 24 hours, for a large constellation of the chosen orbit type. The first two orbit types analyzed were LEO and GEO. Figure 14

shows that while one LEO is capable of detecting objects at large distances from the Earth, the payload cannot detect one-meter objects beyond the halfway point to the Moon.

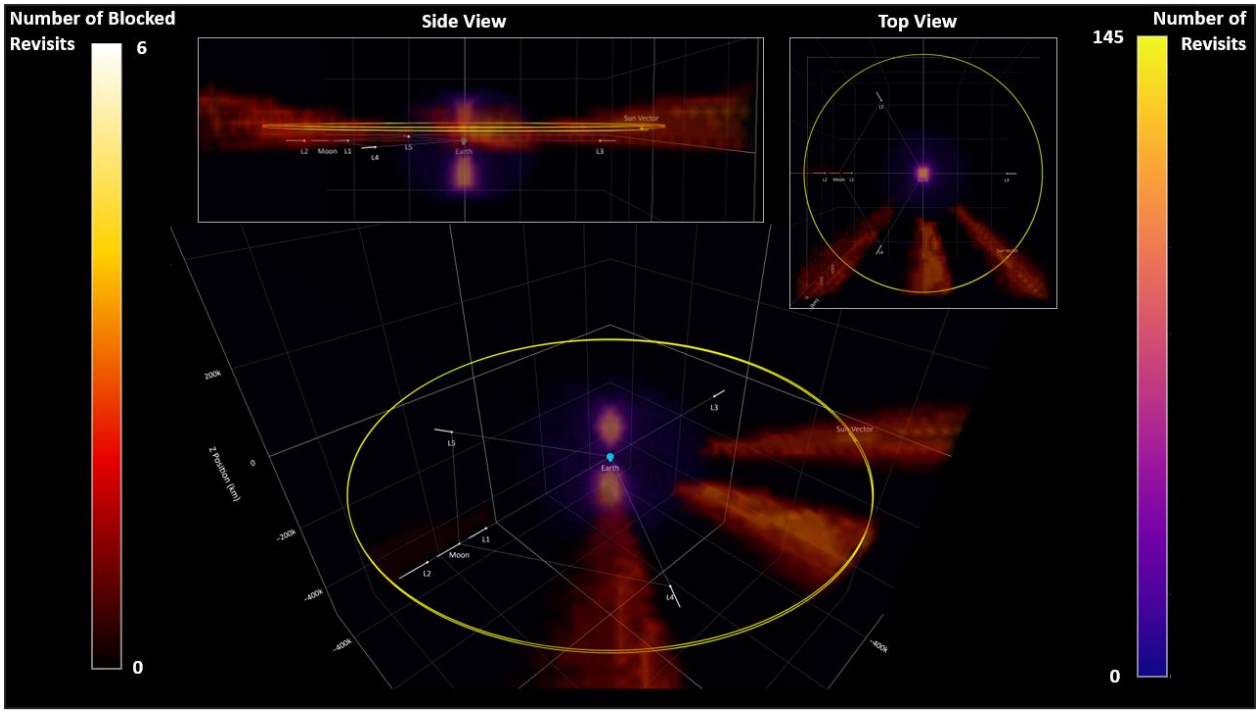

Figure 14: Two Month Detection Coverage Analysis for One LEO Satellite

Figure 15 and Figure 16 depict a similar result. These figures show two different CONOPs for a single inclined GEO. Figure 15 leverages the same CONOPs as the LEO satellite while Figure 16 leverages a 4π Steradian Celestial Sphere Scanning CONOPs. Though the coverage is more evenly distributed because of increased geometric diversity, it does not extend into the full cislunar domain. In addition, there are significant blocked revisits due the Sun, Moon, and Earth.

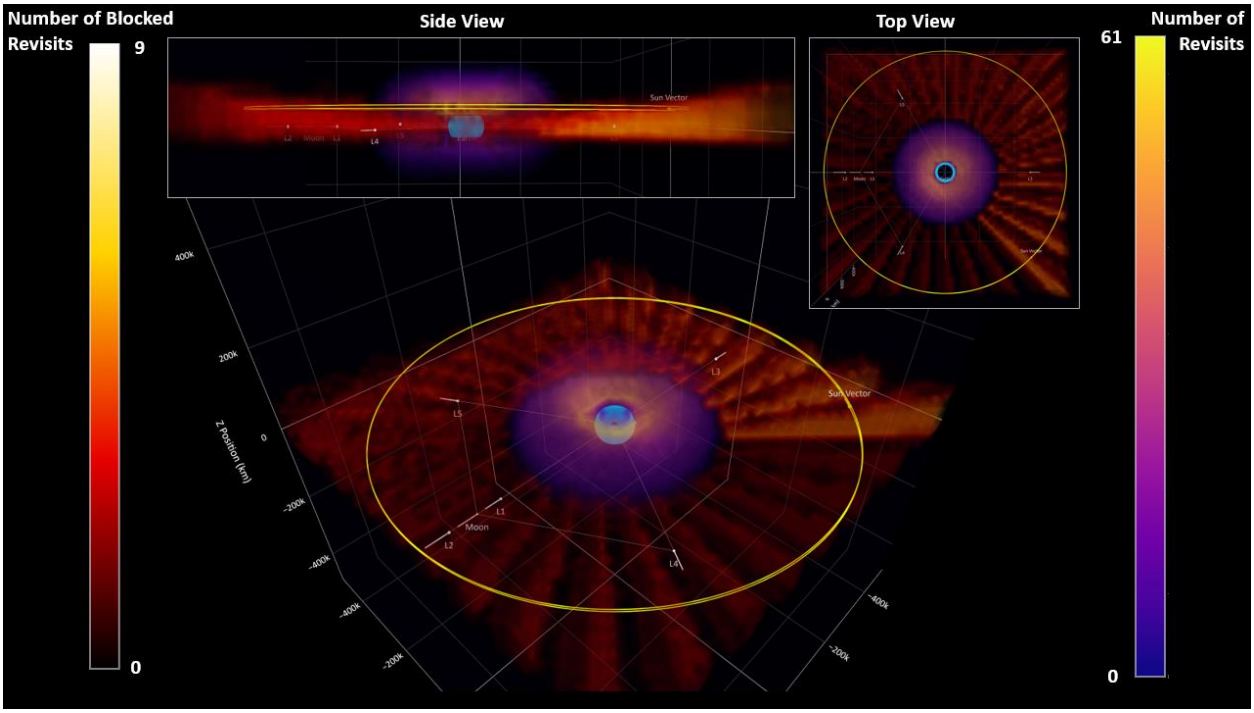

Figure 15: Two Month Detection Coverage Analysis for One Inclined GEO Satellite Scanning in the Velocity Direction

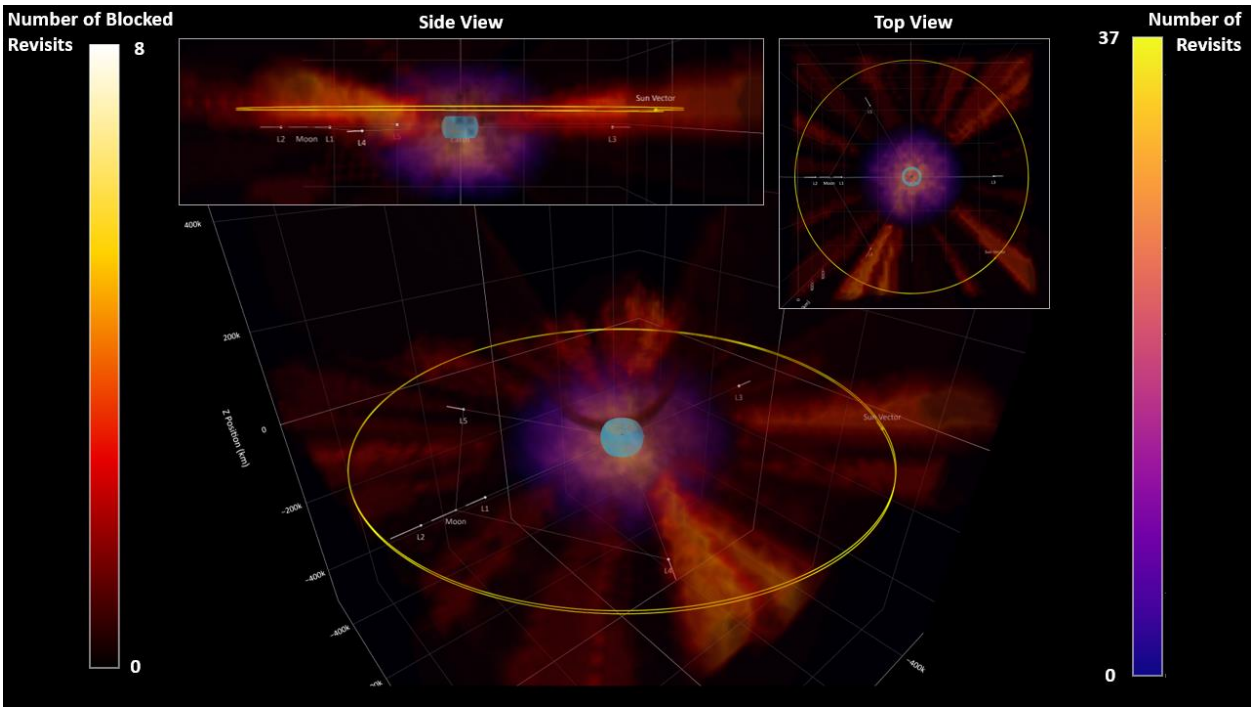

Figure 16: Two Month Detection Coverage Analysis for One GEO Satellite Scanning the 4π Steradian Celestial Sphere

To detect and provide custody further into the cislunar domain, we explored the P/3 lunar resonant orbit. Figure 17 demonstrates the ability of the P/3 lunar resonant orbit to reach further out into the cislunar volume. Due to the

periodic nature of the resonant orbits, there are still regions of the cislunar volume that are not observed at any point by a P/3 orbit.

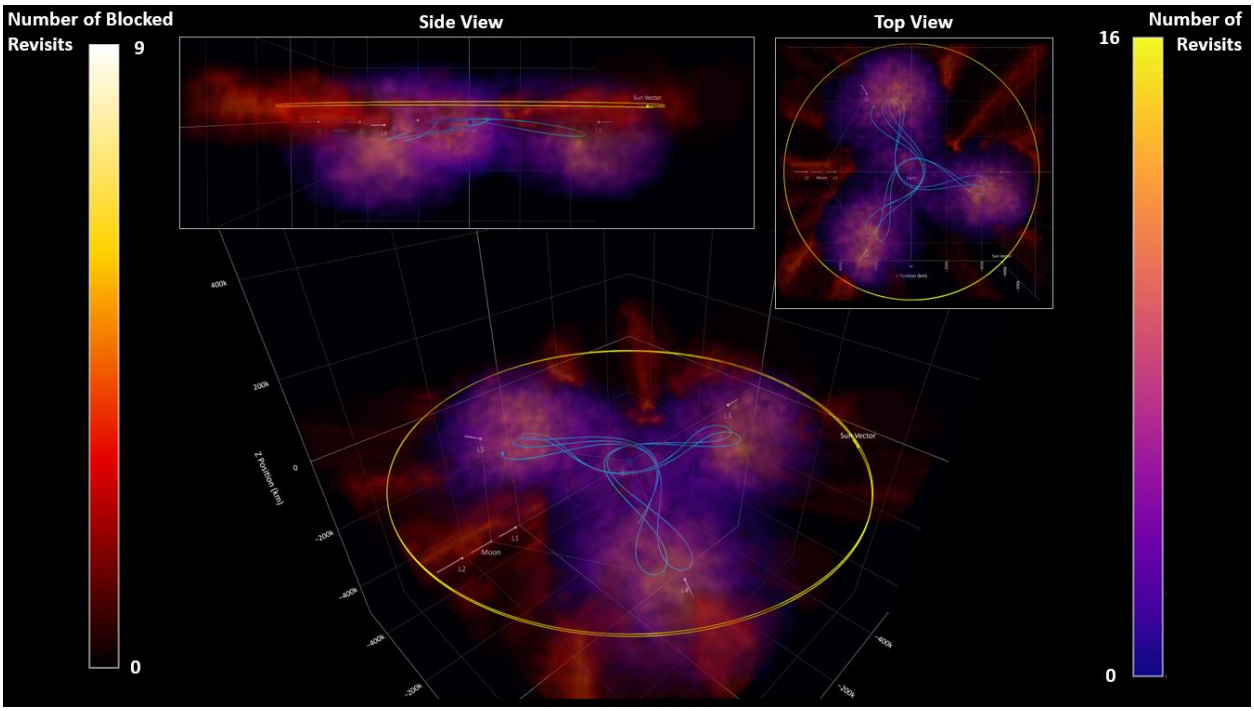

Figure 17: Two Month Detection Coverage Analysis for One Lunar Resonant P/3 Satellite

As a result, other orbit types were also evaluated. Figure 18 shows the results from one satellite at each of the Lagrange points. The results shown in Figure 18 are very intuitive. Each Lagrange point offers 4π steradian coverage at the distances with sufficient SNR for a one-meter diffuse sphere. L1 and L2 offer more revisits in their region due to overlaps in their fields of regard (FOR). While these orbits provide additional geometries for viewing objects of interest, large solar phase angles will make detections difficult around the borders of the domain. For some trajectories, this is a region where small maneuvers can result in large changes to the trajectory, making these regions of high interest for object custody.

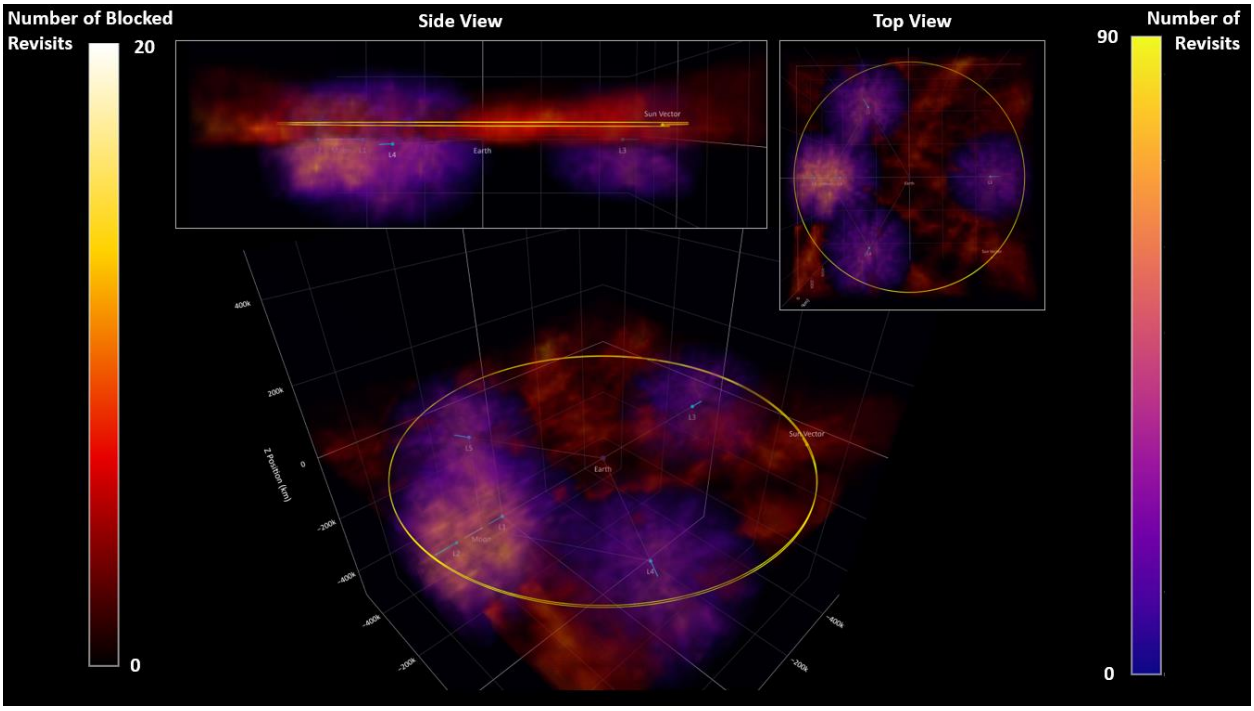

Figure 18: Two Month Detection Coverage Analysis for One Satellite at Each of the Lagrange Points

The final orbit type evaluated was the Chaotic orbit type. These are unstable orbits that are difficult to maintain, requiring significant fuel, however they can cover a more diverse volume of the cislunar space. Figure 19 shows a chaotic orbit that traverses a more diverse region of space. While the diversity is beneficial for detection, it poses significant challenges with respect to orbit stability.

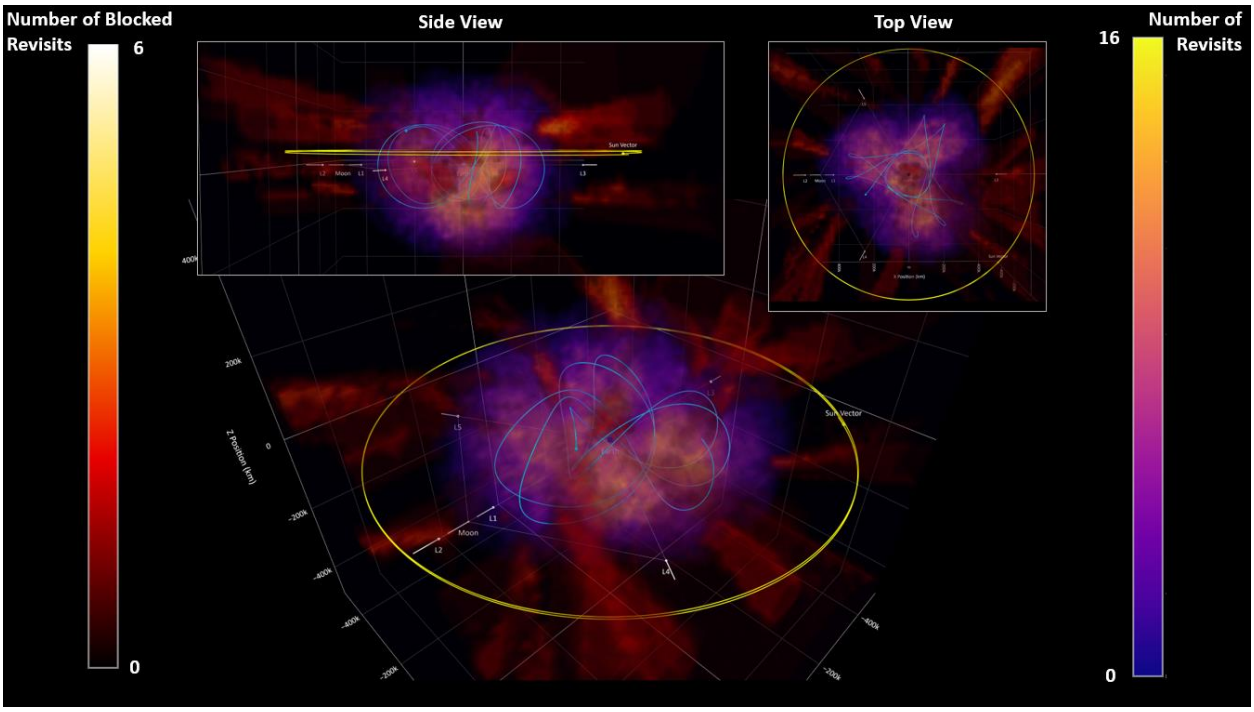

Figure 19: Two Month Detection Coverage Analysis for One Chaotic Orbit Satellite

While the three-dimensional renderings enable detailed qualitative comparisons, it is helpful to simplify the coverage parameters for comparison in a quantitative plot. Figure 20 provides the means to quantitatively view and compare the anticipated coverage of each orbit type.

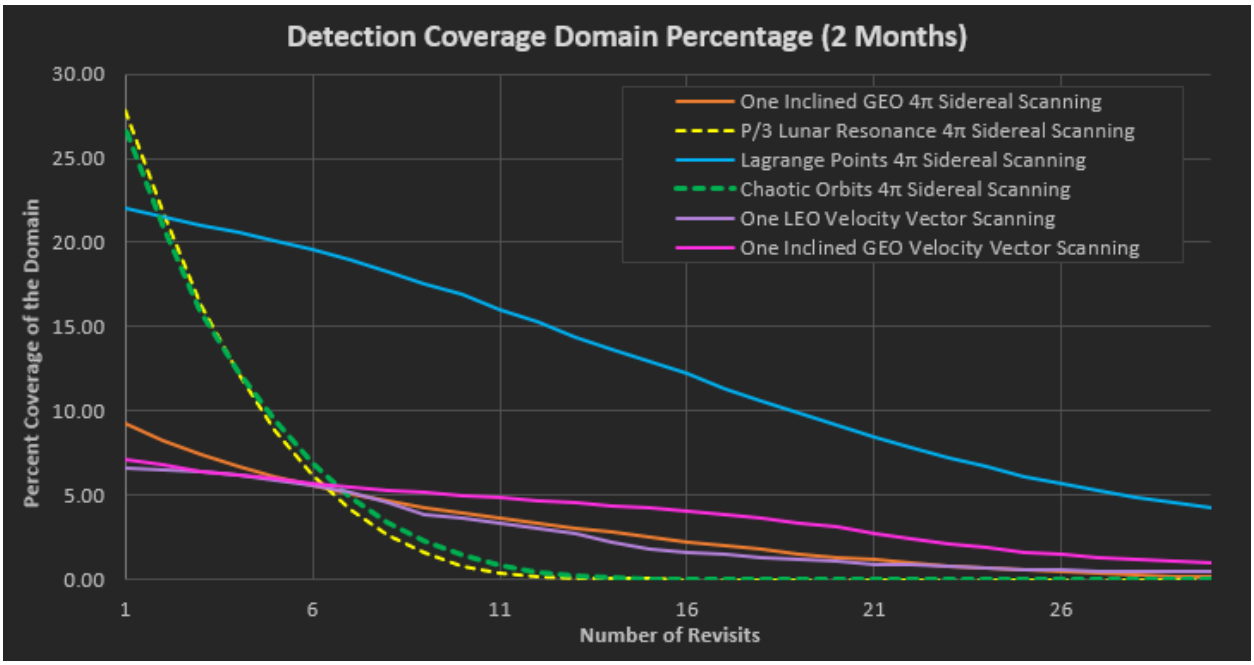

Figure 20: Detection Coverage Domain Percentage Comparison of Orbit Types over a Two Month Period

The single P/3 and Chaotic orbit satellites have the most access to the largest percentages of the domain (27%), which is defined as the 4π steradian sphere around the Earth extending to a radius of 475,000 km. In contrast, the other orbit types with single satellites are all below 10% maximum coverage. As shown in Figure 10, it's possible to increase the number of revisits by adding more satellites to the constellation, but not possible to increase the percent coverage without combining different orbit types. This will be discussed in more detail later in this section. The objective will be to combine different orbit types to design an architecture that meets mission performance needs. Based on the above analysis, 13 different architectures are discussed in this report. Each potential architecture has scaled the number of observer satellites in each of the orbit types as shown in Table 2.

Table 2: Constellation Orbit Type Scaling

Constellation Architectures	Number of Spacecraft per Orbit Type				
	LEO	GEO	Lagrange	Lunar Resonant P/3	Chaotic
LEO Only	75				
GEO Only		24			
Lagrange Only			L1, L2, L3, L4, L5		
P/3 Only				24	
Chaotic Only					24
P/3 & Lagrange			L1, L2, L3, L4, L5	24	
LEO & Lagrange	75		L1, L2, L3, L4, L5		
GEO & Lagrange		24	L1, L2, L3, L4, L5		
GEO & 6x Lagrange		24	6 x [L1, L2, L3, L4, L5]		
GEO, Lagrange, & P/3		24	L1, L2, L3, L4, L5	24	
GEO, 6x Lagrange, & P/3		24	6 x [L1, L2, L3, L4, L5]	24	
GEO, Lagrange, & Chaotic		24	L1, L2, L3, L4, L5		24
GEO, 6x Lagrange, & Chaotic		24	6 x [L1, L2, L3, L4, L5]		24

Each of these potential architectures were modeled over a 24-hour period to assess overall coverage. The results of the domain coverage analysis of these potential architectures is plotted in Figure 21.

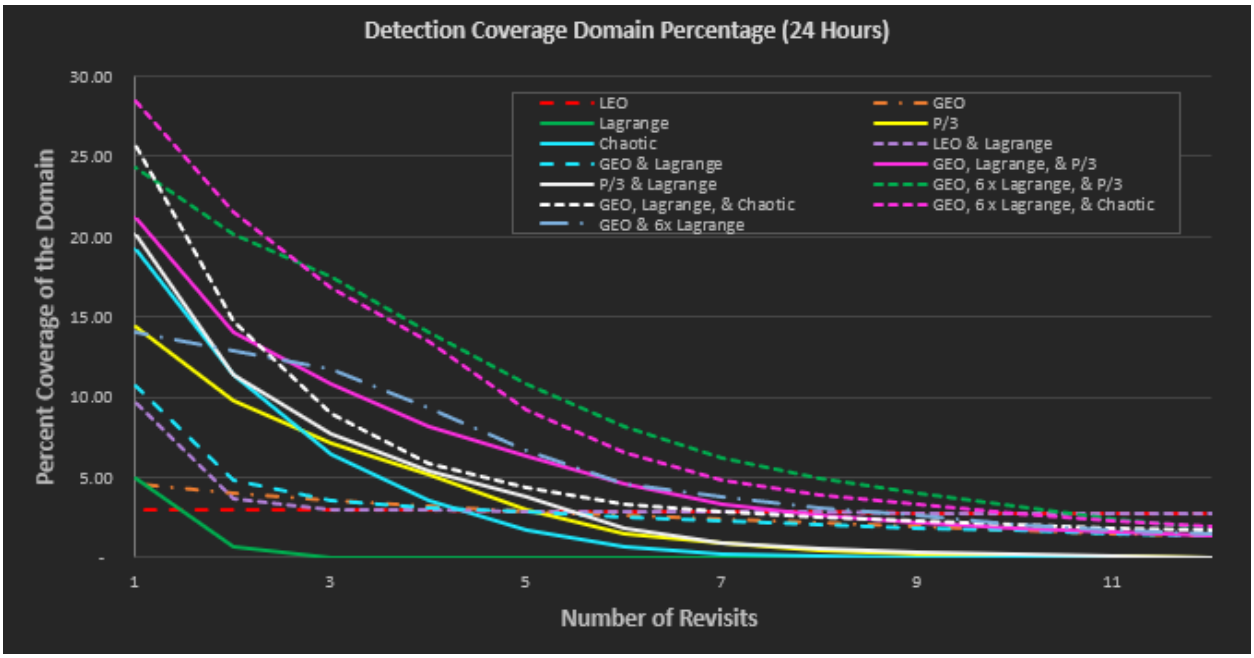

Figure 21: Detection Coverage Domain Percentage Architecture Comparison

While none of the architectures can monitor the entire domain in a 24-hour period, there is a large delta in performance between the LEO based architectures and the Lunar Resonance P/3 based orbits. While the Lunar Resonance P/3 based orbits achieve a higher maximum percentage in coverage, the LEO based architectures achieve

a much higher maximum revisit count. There are very logical explanations for each of these results. The LEO based architecture has many more satellites however they are mostly observing from LEO orbit which provides very little diversity with respect to observing ranges and solar illumination conditions. While the Lunar Resonance P/3 orbits can achieve a significant diversity of measurements, there are fewer satellites over a greater volume, creating less coverage. The plot in Figure 21 provides insight into the advantages and disadvantages of each architecture, while the volumetric histograms provide additional insight into the factors leading to these results. The LEO constellation is an interesting example. In Figure 22 it is apparent that this constellation is entirely blind in the hemisphere centered at the vector from the center of the Earth to the Sun. This is a result of two effects. First, the solar phase angles are too high to generate sufficient SNR for a one meter squared diffuse sphere. In addition, there is a cone of exclusion within that gap excluding the sensor from pointing in that direction.

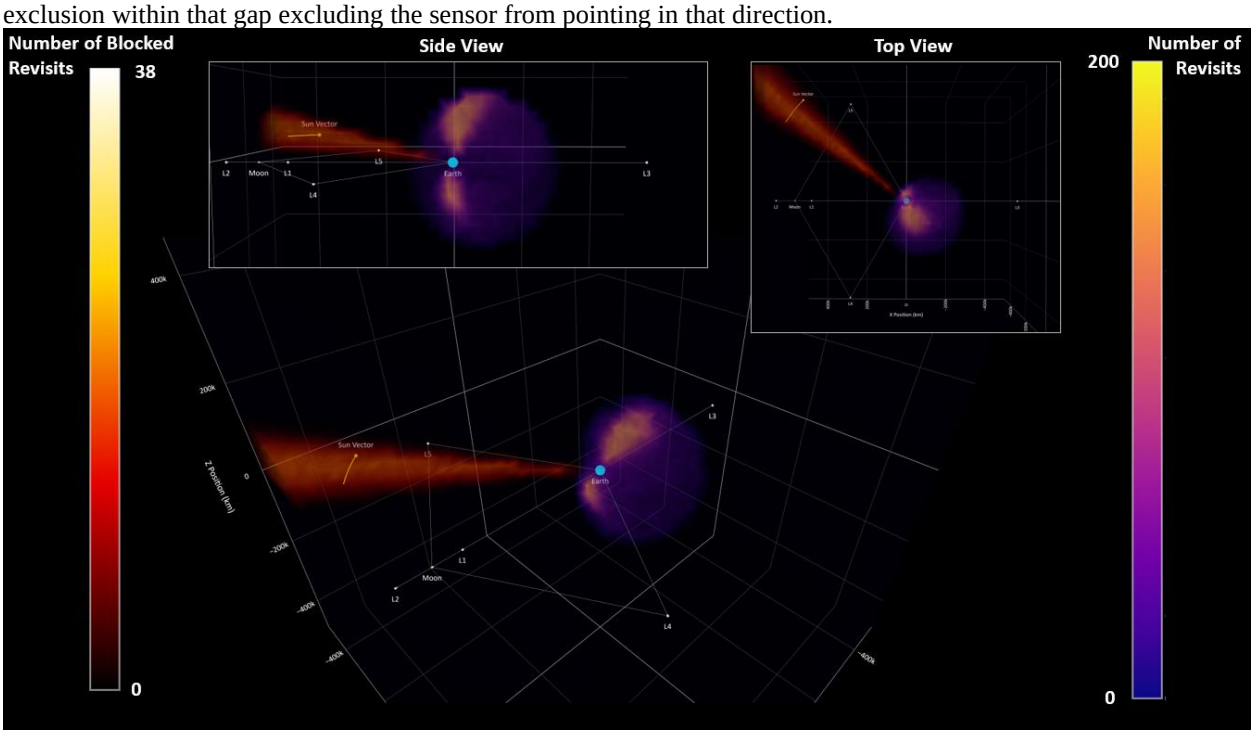

Figure 22: LEO Volumetric Coverage

Migrating to a GEO based architecture with 4π sidereal scanning is shown in Figure 23. This illustrates a more evenly distributed coverage than a constellation of 75 LEOs however it still suffers from the same fundamental challenges: poor solar phase angle diversity and long ranges to target.

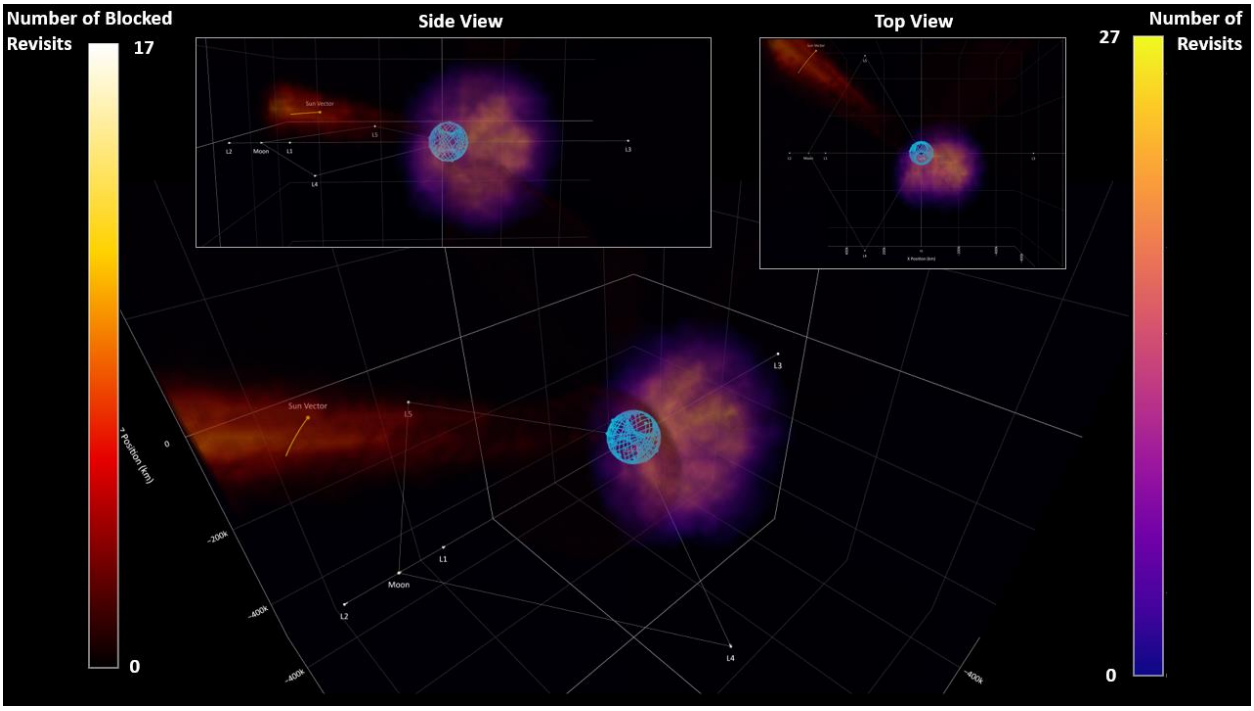

Figure 23: GEO Volumetric Coverage

To increase diversity, observers at each of the Lagrange points were analyzed. In Figure 24 we see that while there is a significant increase in diversity, the region covered by the GEO constellation is now a wide gap.

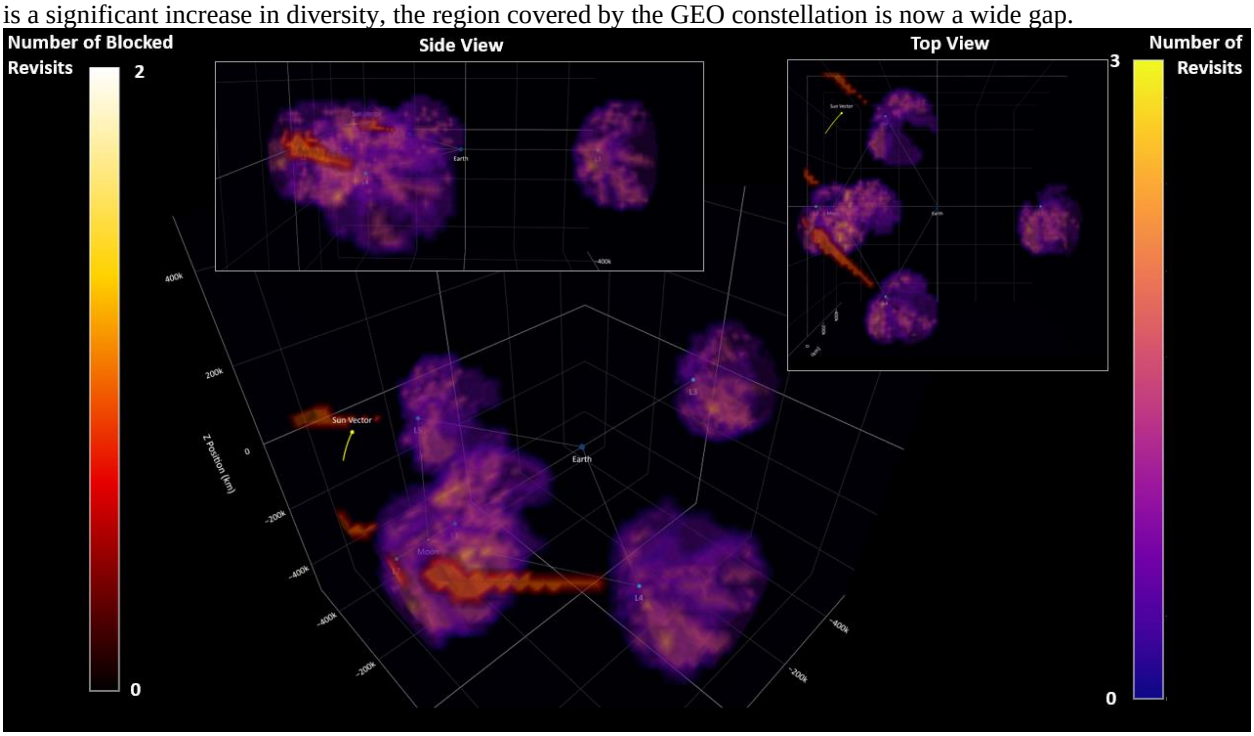

Figure 24: Lagrange Points Volumetric Coverage

To address this gap, we combine the two constellations while increasing to six observers at each Lagrange point to increase the coverage. Figure 25 demonstrates the additional value of the combination of orbit types as opposed to either constellation independently, however there are still gaps in coverage.

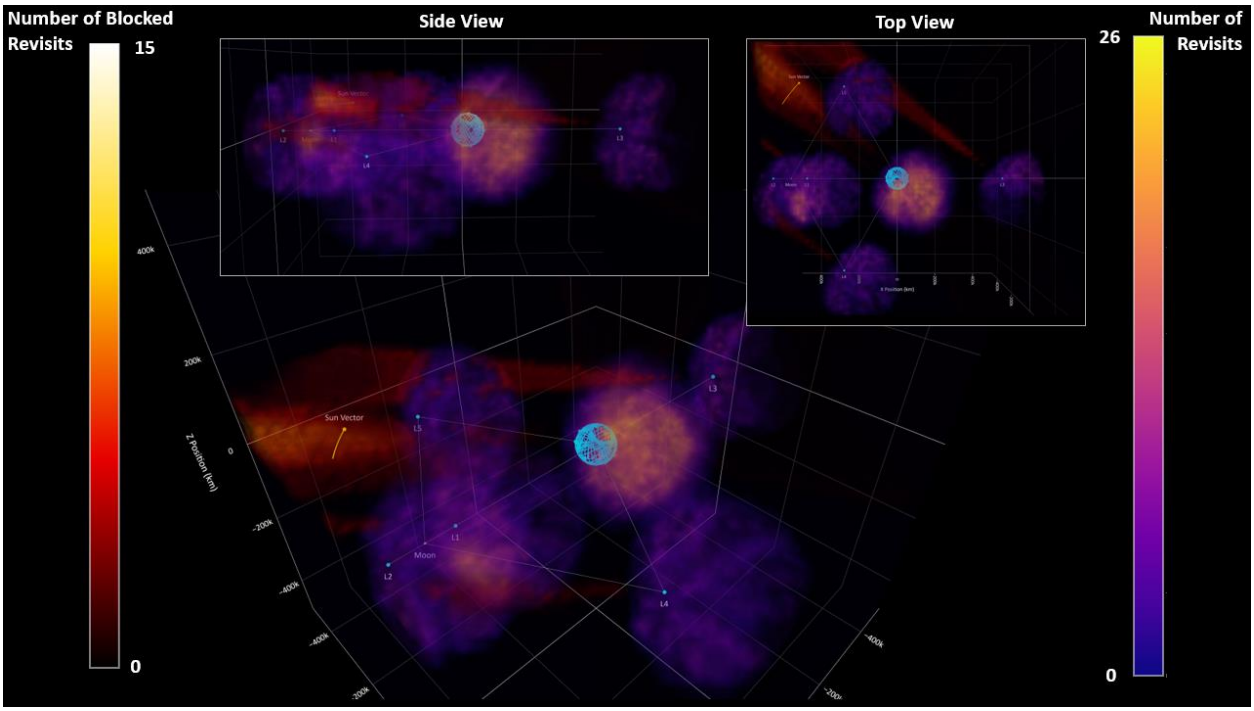

Figure 25: GEOs with 6x Lagrange Points Volumetric Coverage

Figure 26 takes the analysis another step further by adding in the lunar resonant P/3 orbit constellation, which provides some additional improvement. In Figure 26, while some regions in the domain are still not covered, a large percentage of the volume between the Earth and the Moon's orbit is observed in the 24-hour period. This is due to significant diversity in the observing conditions and by combining multiple constellations different strengths and weaknesses with respect to solar phase angle.

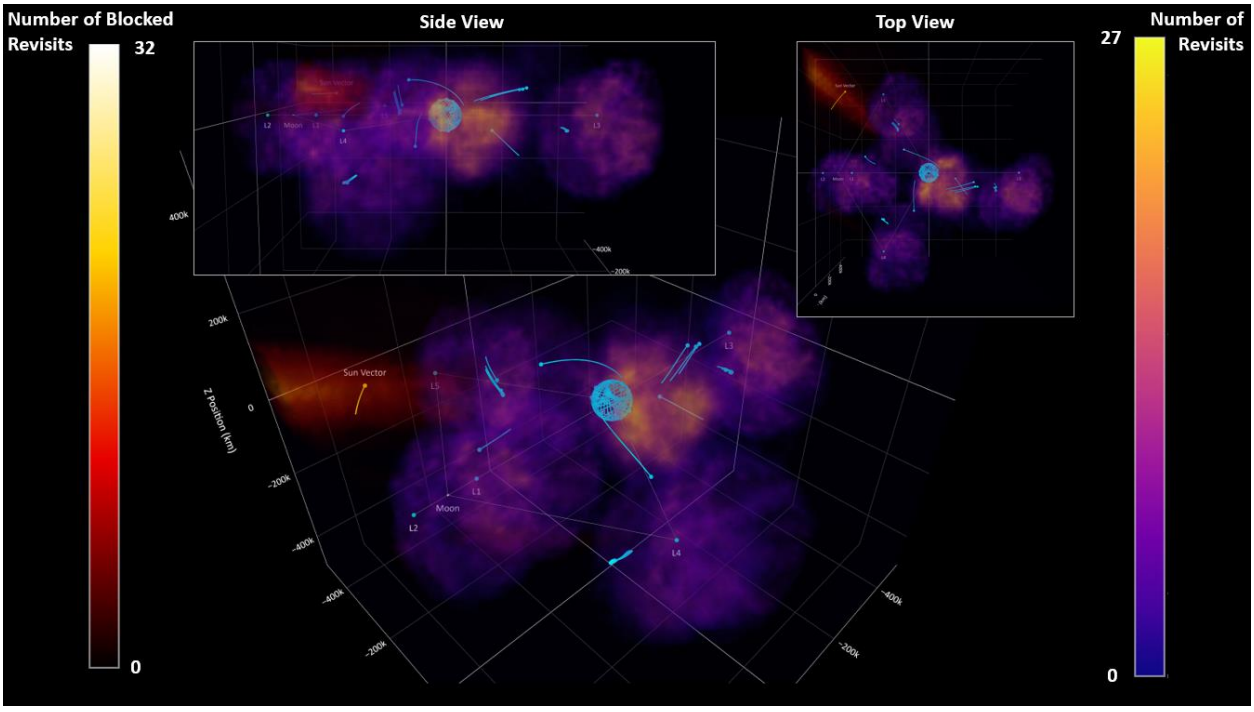

Figure 26: GEO, 6x Lagrange, & P/3 Volumetric Coverage

The next question becomes, which of the architectures is optimal to minimize gaps from a custody perspective? This leads to the next analysis type. The question of custody performance is determined by modeling the architecture design against specific object trajectories. Figure 27 is a three-dimensional rendering of un-cued search of the LEO architecture vs. a free lunar return trajectory during waxing crescent of the Moon. For this discussion, this target trajectory is chosen since it is representative of the most challenging trajectories, primarily due to vast distances and poor solar phase angle conditions. The observing constellation is presumed to know where the object is and attempts to detect the object while tracking in the sidereal frame. While there are a handful of detections in this example, much of the trajectory is not detected with this CONOP.

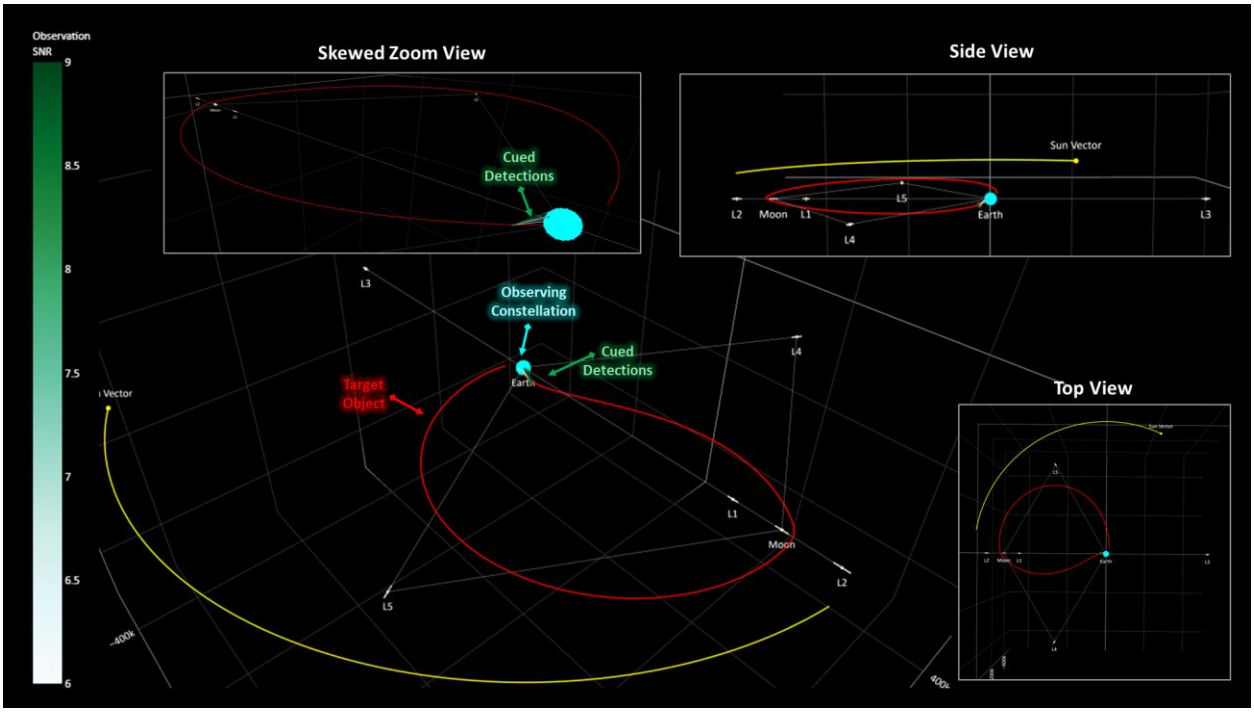

Figure 27: 3D Rendering of a Cued LEO Architecture VS Free Lunar Return during Waxing Crescent

We can also evaluate this scenario by looking at the SNR for any LOS as a function of time. Figure 28 shows that there are only a few detections early in the trajectory, with extremely low SNR for the rest of the trajectory.

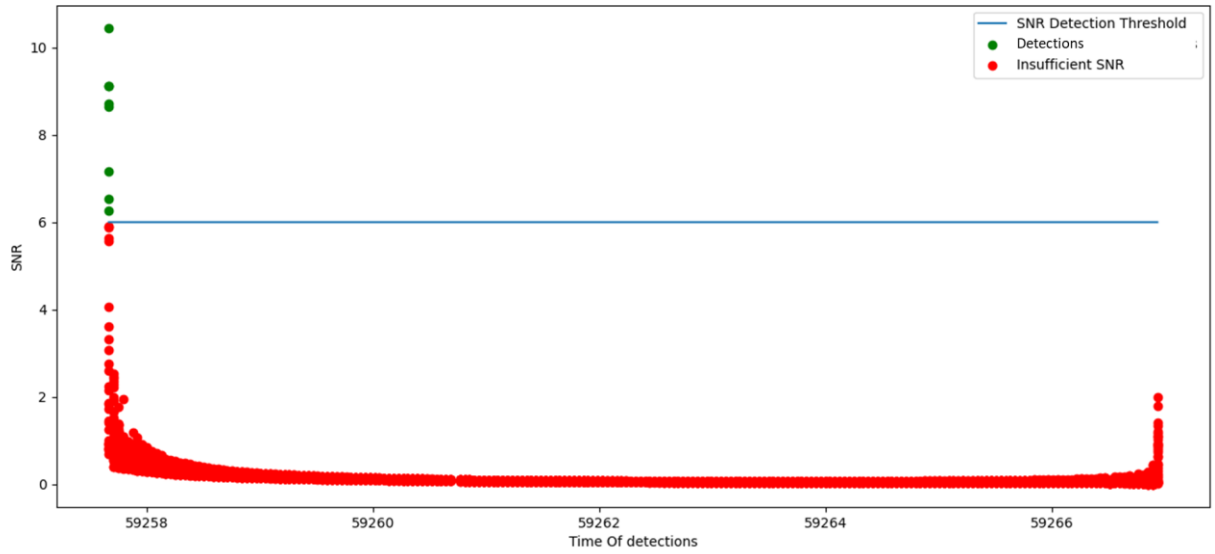

Figure 28: SNR over Time for a Cued LEO architecture VS Free Lunar Return during Waxing Crescent

The next logical step is to attempt to create more observation diversity and decrease the range to target. An incremental approach to this challenge is a migration from the LEO orbit regime to the GEO orbit regime with high inclination orbits. Figure 29 illustrates this architecture's performance.

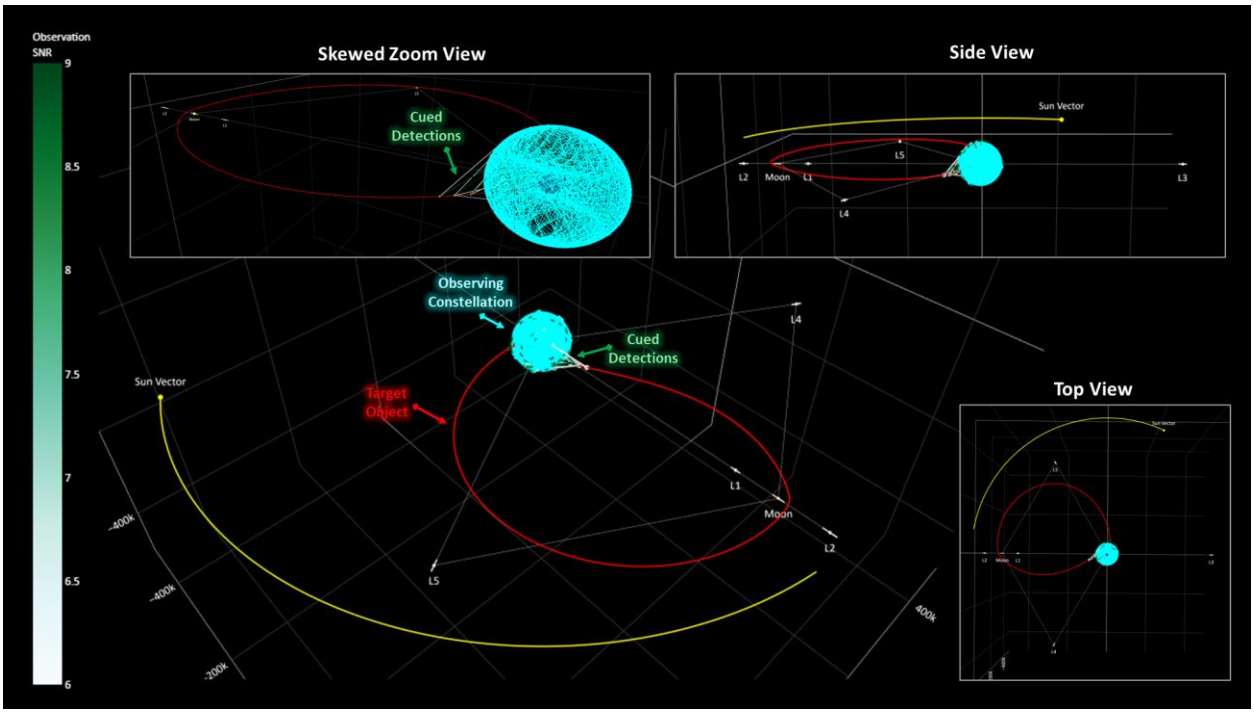

Figure 29: 3D Rendering of a Cued GEO Architecture VS Free Lunar Return during Waxing Crescent

We can see a few detections at the beginning of the trajectory, but there is almost no coverage for most of the trajectory. It is also very difficult to interpret what is happening in the sub GEO regime.

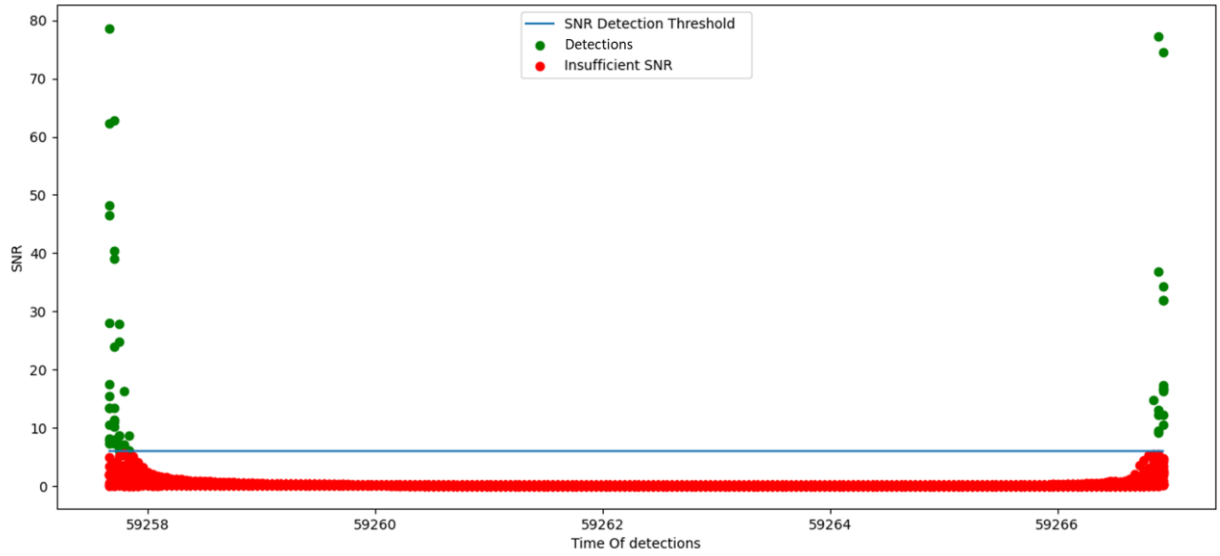

Figure 30: SNR over Time for a Cued GEO Architecture VS Free Lunar Return during Waxing Crescent

Figure 30 gives a better view of the scenario. Not surprisingly we see some improvements due to the increased diversity, specifically, higher peak SNRs and detections at the re-entry point. Still, the object is essentially undetectable for most of the trajectory.

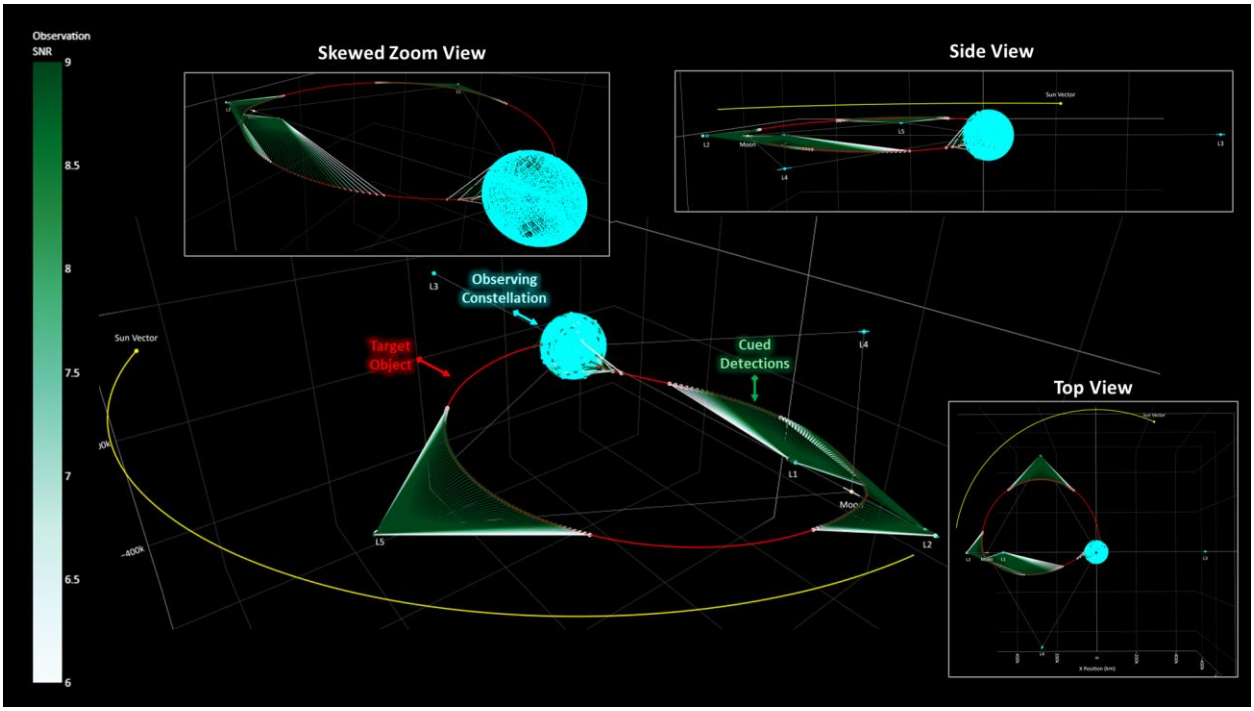

Figure 31: 3D Rendering of a Cued GEO & Lagrange Architecture VS Free Lunar Return during Waxing Crescent

Figure 31 tells a different story. As referenced in Table 2, the GEO & Lagrange Architecture includes five Lagrange orbiting satellites. More specifically, one observer is placed at each of the five Lagrange points. While there are still multiple gaps in custody, these additional geometries substantially improve the overall coverage.

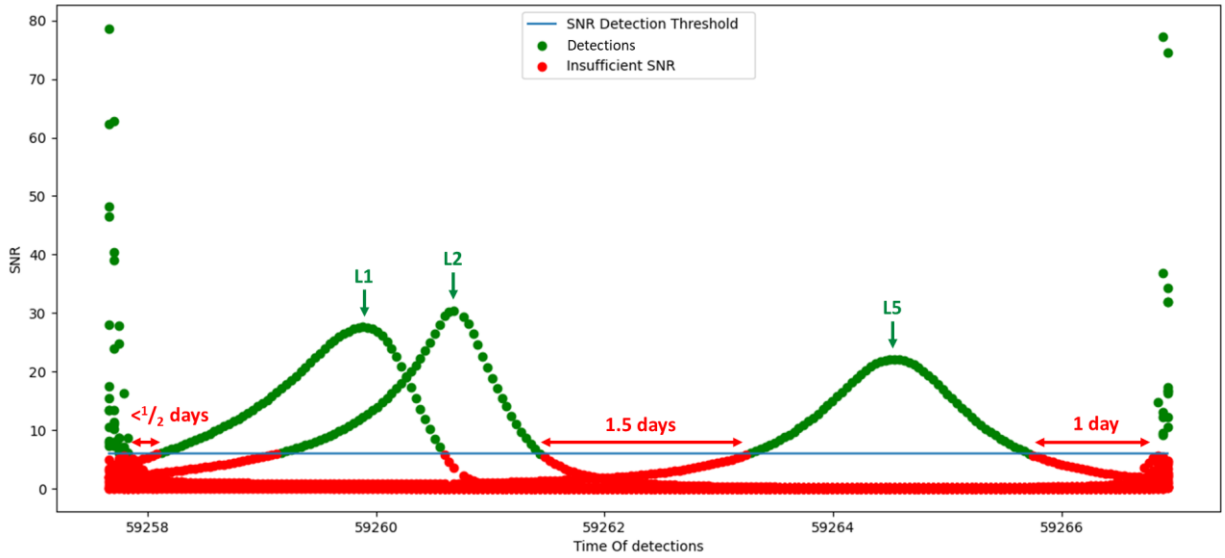

Figure 32: SNR over Time for a Cued GEO & Lagrange Architecture VS Free Lunar Return during Waxing Crescent

Figure 32 plots the gaps of low SNR. They account for approximately three days of the entire flight, providing the object obvious geometries for when to maneuver to avoid reacquisition. In addition, the Lagrange points pose additional challenges for long distance communications without providing full custody. Next, we further attempt to incrementally increase geometric diversity by adding the P/3 lunar resonant orbit class in Figure 33. With the level of diversity, this very quickly becomes a difficult rendering to interpret without 3D interaction.

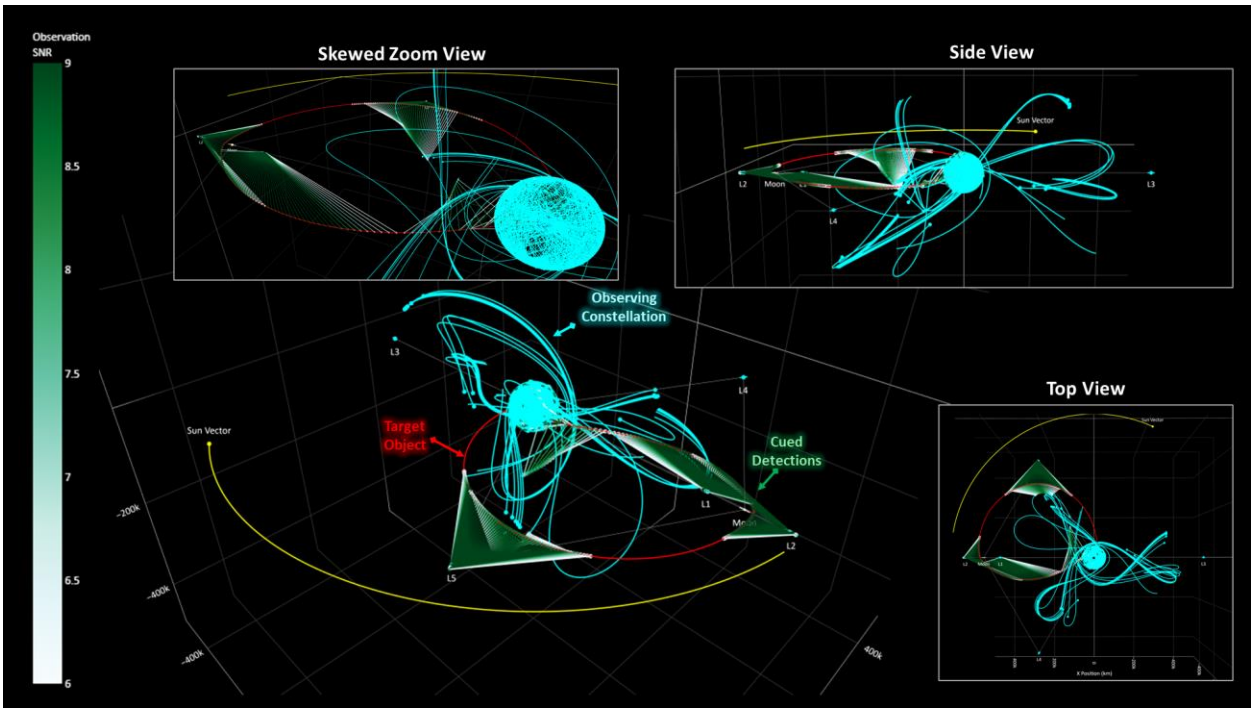

Figure 33: 3D Rendering of a Cued GEO, Lagrange, & P/3 Architecture VS Free Lunar Return during Waxing Crescent

It helps to switch to Figure 34 where SNR for LOS is plotted versus time. Like the other architectures, the object becomes very difficult to detect as the trajectory traverses further into the domain. This is due to both the distance from the observer and the solar phase angle conditions.

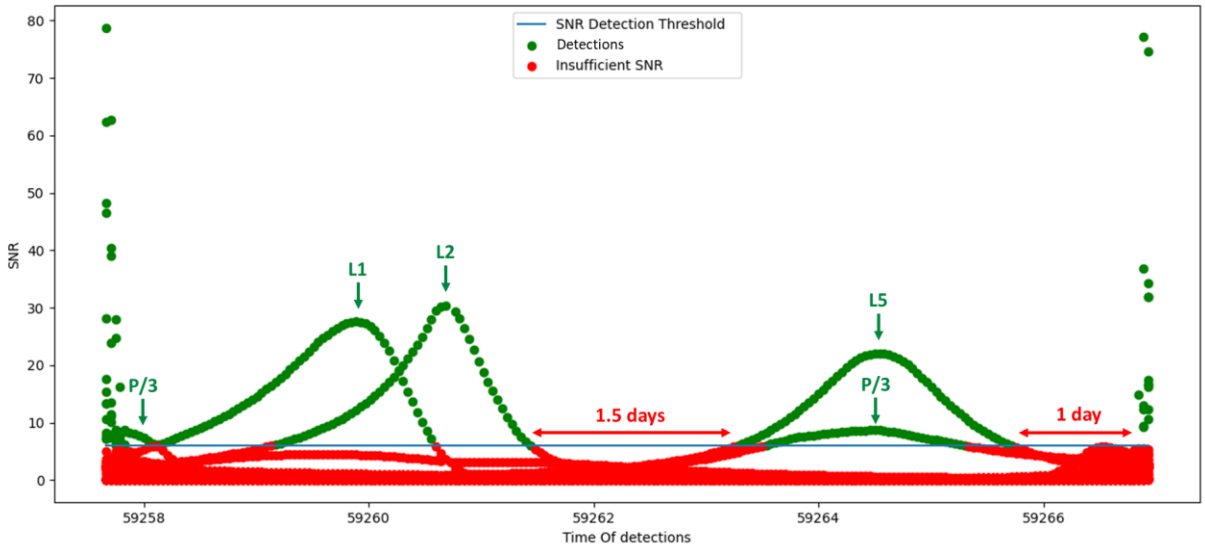

Figure 34: SNR over Time for a Cued GEO, Lagrange, & P/3 Architecture VS Free Lunar Return during Waxing Crescent

The significant gaps in coverage push the architecture to consider unstable orbits like the chaotic orbit class. Figure 35 shows the results from switching from stable P/3 orbits to chaotic orbits. The change creates significantly more observations.

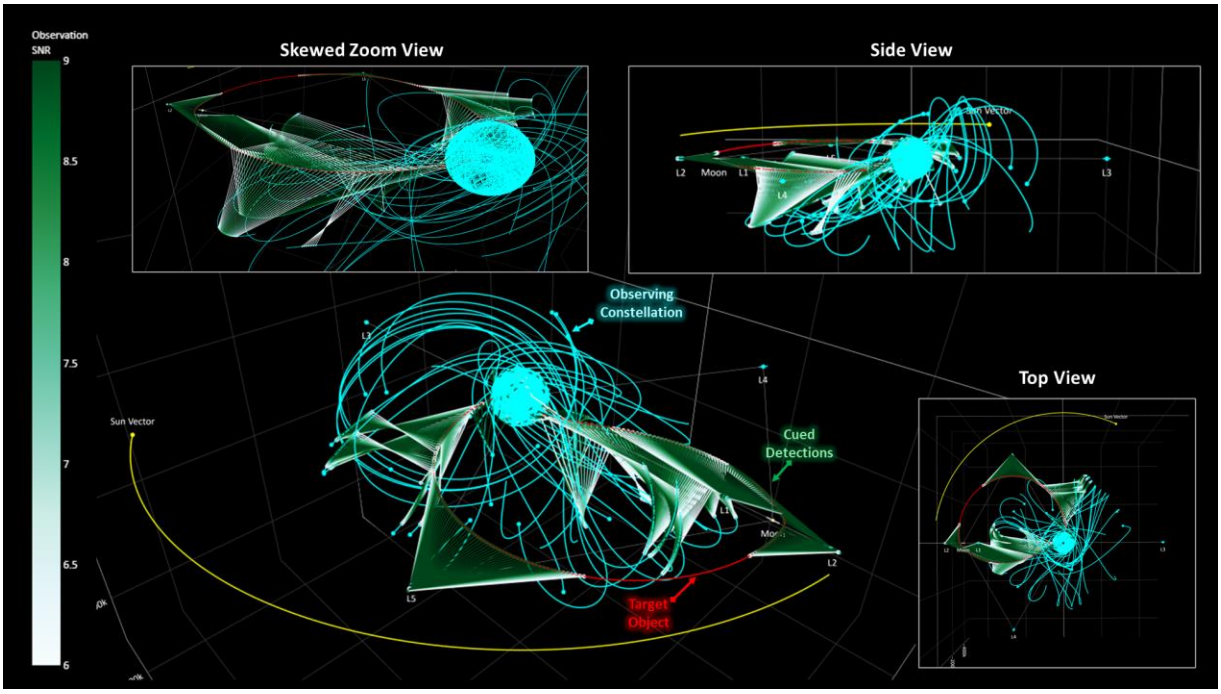

Figure 35: 3D Rendering of a Cued GEO, Lagrange, & Chaotic Architecture VS Free Lunar Return during Waxing Crescent

However in Figure 36 we see that while the 1 day gap at the end of the trajectory has been closed, we still have a gap of 1.5 days. To close this gap another approach will be necessary. Either another orbit class, sensing phenomenology, or a highly maneuverable satellite capable of maintaining a close distance while maintaining the necessary solar phase angle conditions.

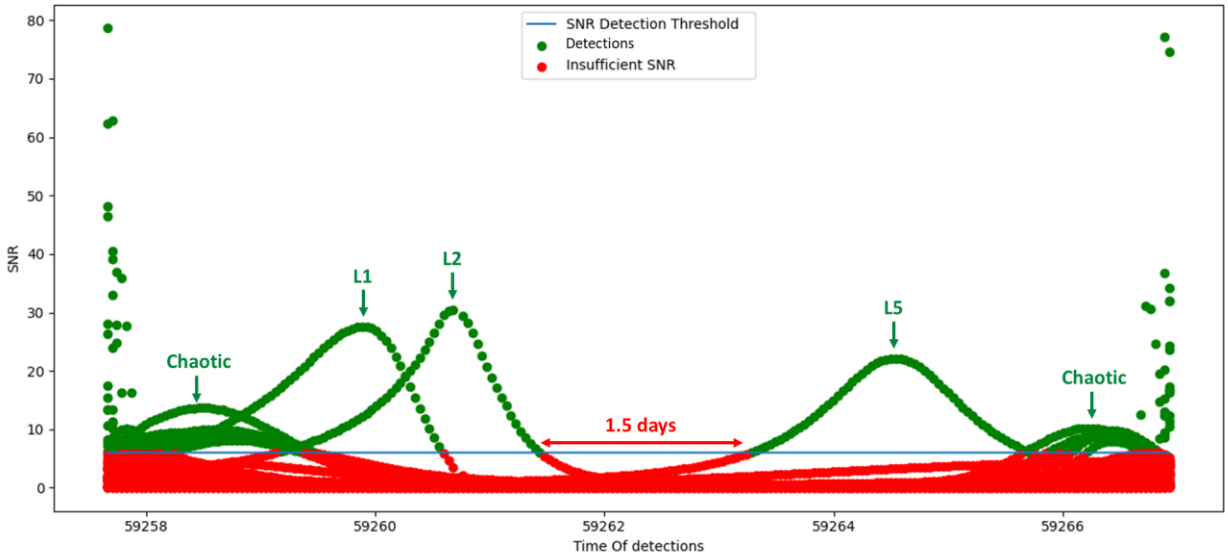

Figure 36: SNR over Time for a Cued GEO, Lagrange, & Chaotic Architecture VS Free Lunar Return during Waxing Crescent

These detailed custody analyses can be effectively summarized in a simple timeline of effective custody comparison. This is shown in Table 3.

Table 3: Modeled Architectures Effective Custody

Constellation Architectures	Days From Launch																				
	0.0	0.5	1.0	1.5	2.0	2.5	3.0	3.5	4.0	4.5	5.0	5.5	6.0	6.5	7.0	7.5	8.0	8.5	9.0	9.5	10.0
LEO Only																					
GEO Only																					
GEO & Lagrange																					
GEO, Lagrange, & P/3																					
GEO, Lagrange, & Chaotic																					

No Custody
Single Observer Low SNR Custody
Multi Observer Low SNR Custody
Single Observer High SNR Custody
Multi Observer High SNR Custody

The evaluated architectures discussed in this paper are not capable of providing persistent custody during the entire trajectory. With multiple orbit classes it is possible to achieve persistent coverage with a 42 cm optical aperture except during the most challenging 1.5 days. The diverse geometries achieve the solar phase angle diversity necessary to detect the one-meter squared object during the rest of the trajectory. The most effective architecture is a combination of three constellation orbit classes: GEO, Lagrange points, and chaotic orbits however both the Lagrange points and the chaotic orbits present significant challenges for observer constellation orbit stability.

5. OBSERVING CONSTELLATION ORBIT STABILITY

The cislunar orbit trade space for the three-body Earth-Moon-observer is complex. This is due to the gravitational forces applied to the observer's orbit within the cislunar volume, specifically, the relationship between the observer's location and the Moon. The Moon's gravity has the potential to make observer's orbit chaotic in nature to include high swings in orbital parameters, specifically inclination, apogee, and perigee values. In some cases, if not properly monitored and controlled, the lunar gravity can create an Earth reentry scenario. The Moon's gravity also

has the potential to induce orbit stability as well. The best example of these locations are the Lagrange points, see Figure 3, specifically, the L4 and L5 points which are extremely stable. Additionally, there are multiple families of periodic orbits including Halo orbits around the Lagrange points.

An orbit's stability or lack thereof can have significant impacts on the mission design (e.g. fuel utilization/need) or mission design life. To fully understand an orbit's stability, analysis needs to occur over the course of the mission's operational lifetime, typically measured in years. The impact of the Earth-Moon system on an orbit is observable over the mission duration. Figure 37, Figure 38, and Figure 39 illustrate the impact on the orbit's apoapsis, periapsis, and inclination due to the Earth-Moon system for the chaotic and stable (P/3) orbits. Figure 37 and Figure 38 show the altitude of apoapsis and periapsis in Earth radii (Re) for the two orbits, respectively. While there is variation in both the apoapsis and periapsis for both the chaotic and P/3 orbits, the chaotic orbit has significant changes. The apoapsis amplitude for the chaotic orbit is approximately 10 Re. The P/3 orbit has an maximum amplitude of 2 to 3 Re. Figure 38 shows similar trends, as expected, for the periapsis values.

In Figure 38, is it important to note that the starting periapsis altitude is approximately 7.5 Re, well above the GEO belt. Over time the periapsis altitude value drops to approximately 3.5 Re, within the GEO belt and potentially in the vicinity of MEO and HEO constellations and orbits. While all objects should be screened for conjunction assessment, the predictability of the P/3 orbit and provides confidence that there is very low risk for a conjunction to occur. This is due to the spacecraft population density beyond GEO. The same cannot be said for the chaotic orbit. While still likely rare, conjunction screening and associated location uncertainty are more important to understand as the chaotic orbit enters space more heavily populated by operational spacecraft. As a result, mission designers and operators need to account for the increased analysis to determine if conjunctions exist and the associated activities to avoid conjunctions. This can be in the form of maneuver to avoid individual events or trajectory planning to ensure the spacecraft remains away from locations where other spacecraft may operate (e.g. stays above the GEO belt). In some cases, as with the IBEX mission [17], the change in periapsis altitude may cause mission life issues. This was one of the reasons why IBEX changed from a chaotic orbit to the stable P/3 orbit.

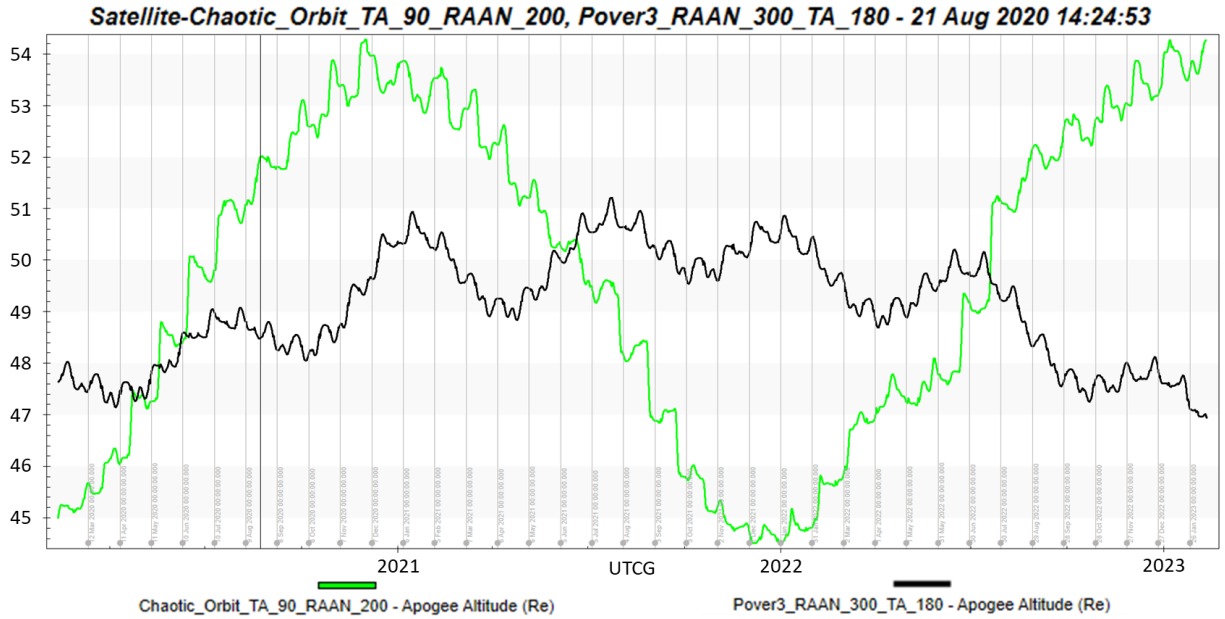

Figure 37: Apoapsis Altitude in Earth Radii over 3 Years, J2000 Reference Frame - Chaotic (Green) & Stable (Black) Orbits

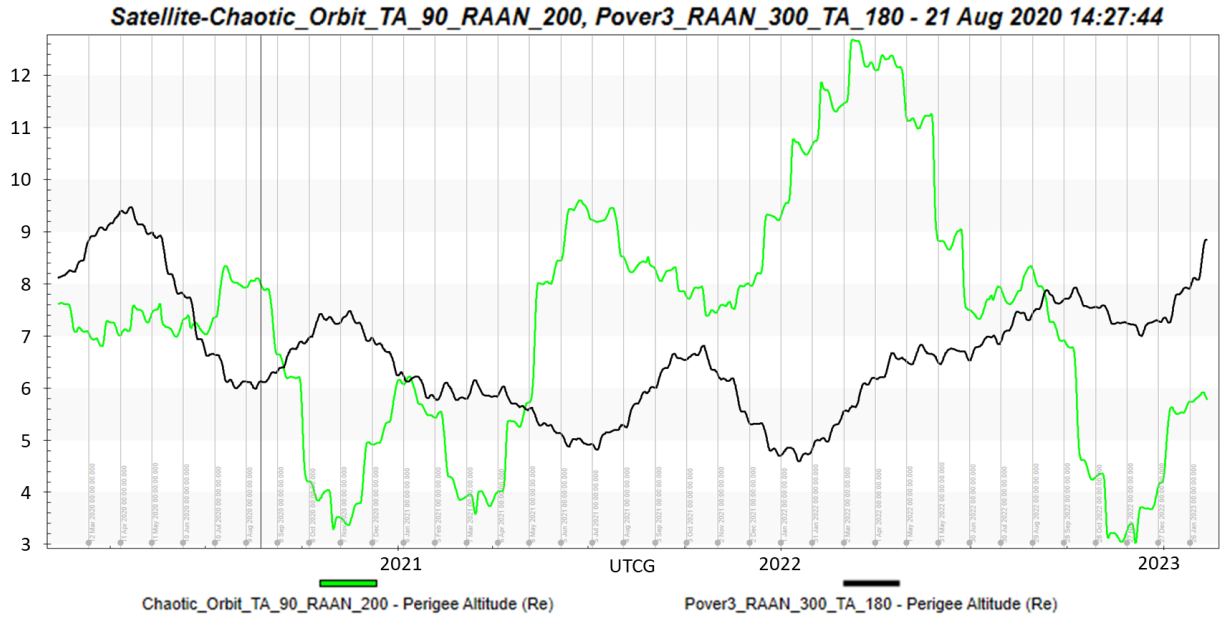

Figure 38: Periapsis Altitude in Earth Radii over 3 Years, J2000 Reference Frame - Chaotic (Green) & Stable (Black) Orbits

Figure 39 and Figure 40 showcase the impacts of the Earth-Moon system for a spacecraft in Earth orbit but operating in the cislunar volume. From Figure 39, the inclination for the chaotic system changes wildly over time, all due to the spacecraft's position with respect to the Moon. There are typically large changes in the inclination value and are a result of the spacecraft's proximity to the Moon. The large changes occur when the spacecraft is at or near apogee and at or near periselene. As spacecraft's apogee location rotates away from the Moon due to the spacecraft and Moon's orbit the change in inclination is relatively small. The large changes in inclination also cause a non-planar effect on the orbit, shown in Figure 41. While this can be accounted for with numerical propagation and a full-force model there are downstream impacts. Typically, tracking stations are provided with Two Line Element (TLE) sets to point antennas for communication windows. TLEs need to be evaluated for their accuracy during periods of time when non-planar situation occurs. This typically results in multiple TLEs being delivered which are only valid for specific time intervals.

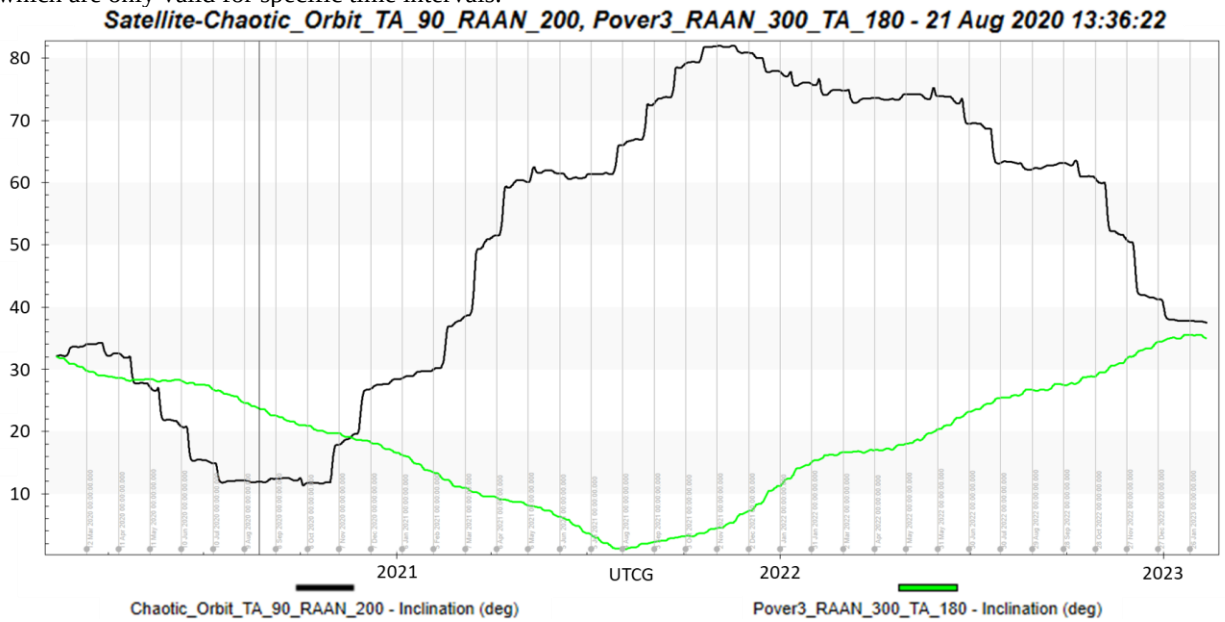

Figure 39: Inclination in Deg over 3 Years, J2000 Reference Frame - Chaotic (Green) & Stable (Black) Orbits

Figure 40, specifically the right picture, illustrates the difference between the chaotic orbit (yellow) and a stable orbit (cyan) from a trajectory perspective. The chaotic orbit changes significantly over time in the Earth-Moon Rotating frame where the P/3 orbit is very predictable. In this example the P/3 spacecraft is in one of the three "propeller" blades at any given time. In this case the spacecraft spends approximately 9 days in each blade. This is a positive when trying to track and communicate with the spacecraft and predict where it will be at any given time. Additionally, the stable orbits are stable for years. When IBEX entered the P/3 orbit in 2013, it was estimated that it would remain in this orbit for at least 50 years, if not longer.

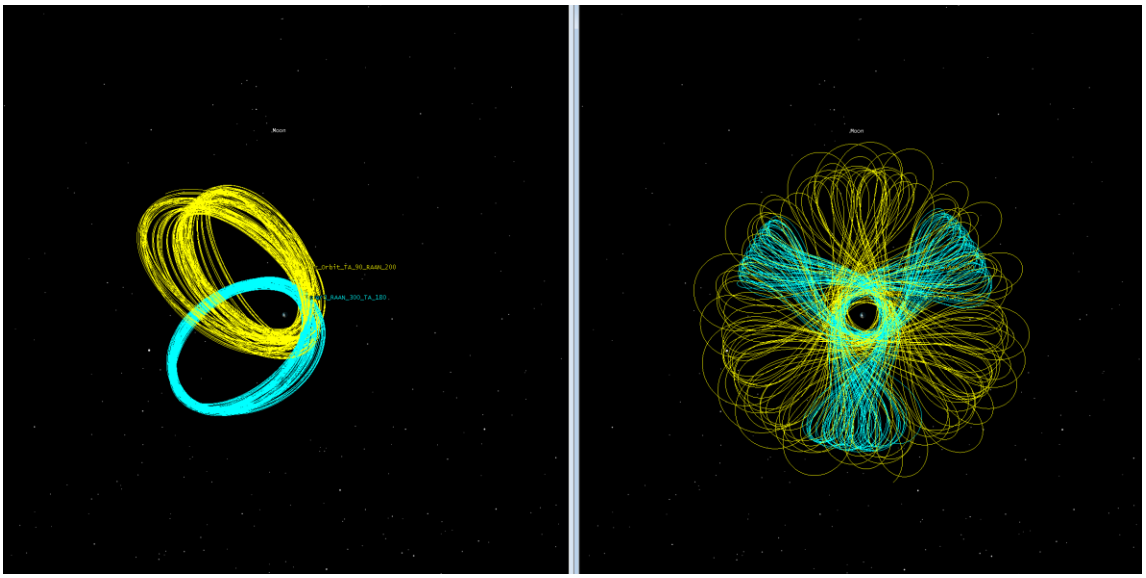

Figure 40: Orbit Comparison Between Viewing Reference Frames – J2000 (Left), Earth-Moon Rotating (Right)

Figure 41: Moon's Gravity Causing Non-Planar Effects on Chaotic Orbit

From the analysis above, the Earth-Moon environment is complex and requires multiple factors to be evaluated and analyzed over the entire mission duration. This includes proper modeling and visualization of the environment. Without this analysis, improper decisions and design choices could be made that significantly impact the success of any mission.

6. TOO SHORT ARC PROBLEM

The Too Short Arc (TSA) problem occurs while attempting to track unknown objects in orbit about the Earth or in the solar system (i.e. asteroids or space debris) where conditions limit the ability to construct a complete orbital solution. Tracking objects in the cislunar domain also comes with limiting conditions (very large ranges and poor illumination) which result in too short intervals of suitable information gathering for typical orbit determination.

To address the TSA problem, many begin with defining an admissible region for a set of observations. [18] presents the concept of an admissible region to confine the set of possible range (ρ) and range-rate ($\dot{\rho}$) values to track asteroids from an Earth-based observer. [19] and [20] generalize the problem to objects in geocentric orbits with Earth-based observers, while [21] further expands the problem to include space-based observers from LEO and GEO. Determining an admissible region for either a ground- or space-based observer to the cislunar domain proves to be more difficult because of the possibility of incorporating three-body dynamics.

For example, consider the observation of an object on a lunar free return trajectory by a satellite in one of the previously described constellation architectures. Because the target object is influenced by gravity from both the Earth and Moon, typical constraints related to equations describing two-body dynamics, such as specific orbit energy or the radius at periapsis/apoapsis, will not apply.

Because of this, we chose to instead limit the possible set of [ρ, $\dot{\rho}$] by investigating the geometric diversity introduced by the candidate observer constellations. For this analysis, the range and range rate are analyzed in the J2000 ECI reference frame where range and range rate are relative to the center of the Earth for the spacecraft to be tracked. Since the observers are constellations of satellites potentially distributed throughout the domain, it was necessary to define the coordinate frame independent of any of the satellites.

To perform the analysis, the domain was defined as a cube centered at the Earth's center in the J2000 frame. Each side of the cube is 1,000,000 km. It was then quantized in each dimension 150 times to create 3,375,000 reference points distributed evenly throughout the domain definition. For each constellation, two time-steps were modeled at one hour apart for each observer performing cued tracking vs the free lunar return trajectory during waxing crescent. Each reference point recorded the number for sensors observing the reference point while tracking the target. A field of view with 1 degree was simulated. This FOV size was chosen to illustrate the key concepts of uncertainty. Ideally the FOV would have been modeled at a representative uncertainty of a system (likely measured in arcseconds), however the domain would have required 1,000,000,000 more reference points. With the computational resources available for this paper, that is not possible, so the field of view was increased to effectively demonstrate the key concepts for the TSA evaluation.

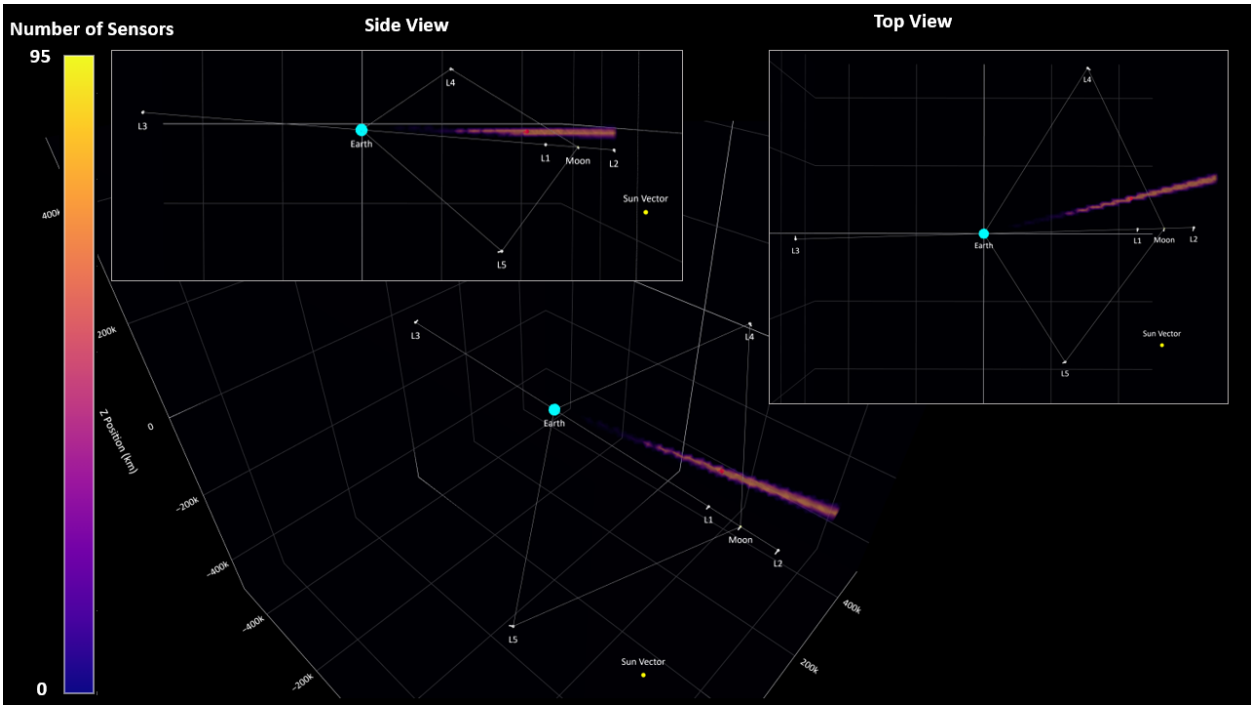

Figure 42: LEO Constellation Uncertainty Rendering

At each time step, the reference points describe the volumetric uncertainties given a specific constellation. These can be rendered like the SNR volumetric analysis that was described earlier in the paper. Figure 42 illustrates the case of 75 LEOs and the distribution created by their overlapping fields of view. By analyzing the distributions at two different time steps, the possible ranges and range rates can be computed with each reference point's contribution to the uncertainty volume weighted by the number of sensors with access to that reference point while pointed at the target. The candidate ranges and range rates are then down sampled by only analyzing the reference points within the top 20% revisits. Stated more simply, the points are filtered down to only the top 20% points which correspond to the yellow region in the cone. This is more apparent in Figure 43.

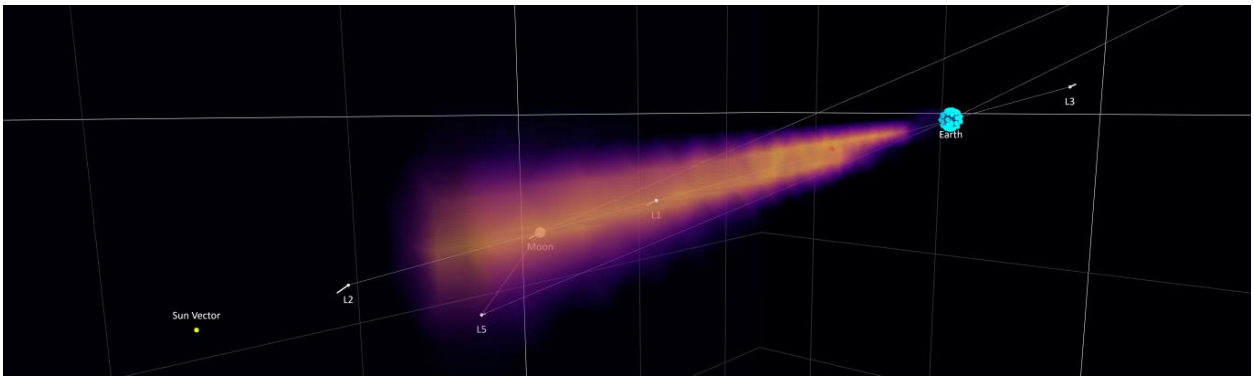

Figure 43: Skewed View of the Uncertainty Volume

We can then fit a weighted Gaussian KDE [22] to the range and range rate distributions to view the resultant uncertainties with consistent 2D metrics. The potential range rates are constrained to having a magnitude less than twice the escape velocity of Earth, i.e. < 22.4 km/s.

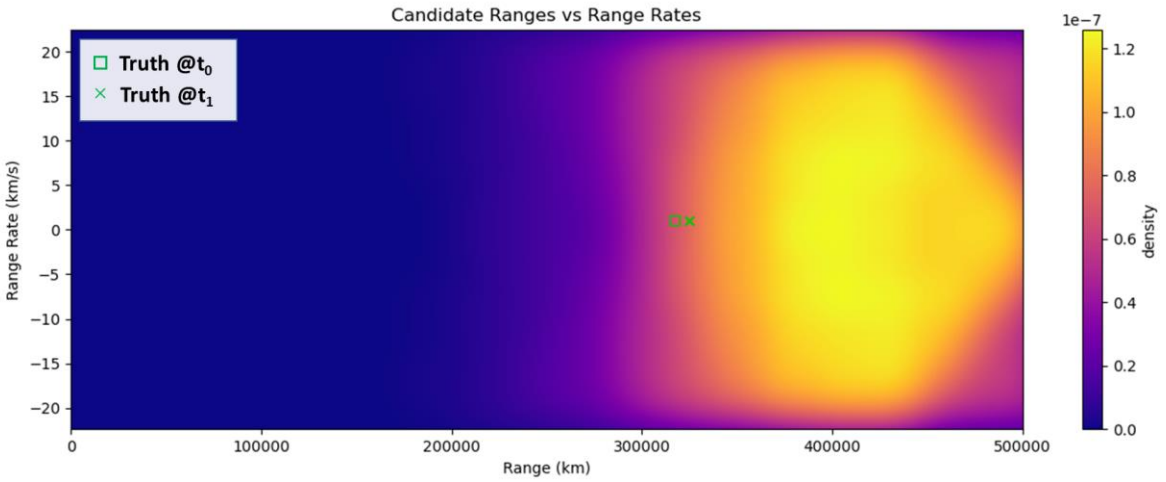

Figure 44: LEO Constellation Range vs Range Rate Uncertainties

Figure 44 plots the associated constrained uncertainties for the LEO constellation over a one-hour period. It is very apparent that while the uncertainty area contains the object of interest, the resultant uncertainty provides very minimal value over an hour with one-degree resolution from a LEO constellation.

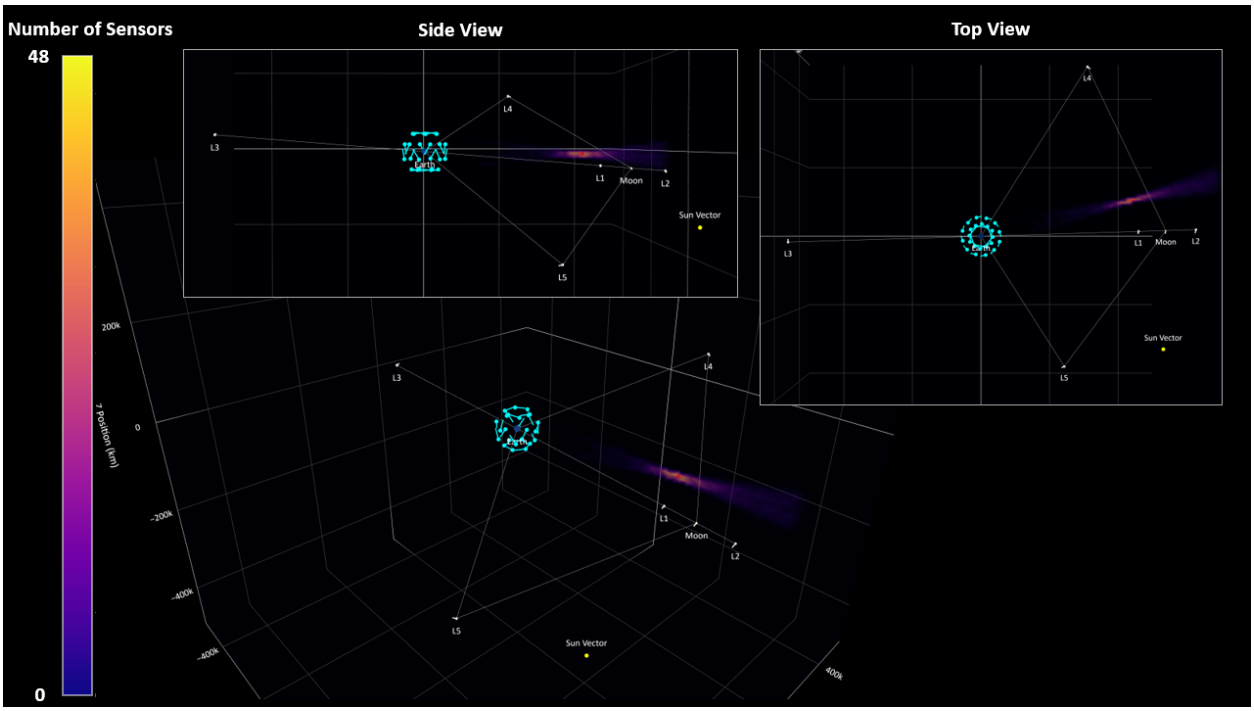

Figure 45: GEO Constellation Uncertainty Rendering

Figure 45 illustrates the same uncertainty rendering for the previously presented inclined GEO constellation. It is apparent that the overlapping FOVs create a region of dense coverage surrounding the free lunar return trajectory. This contrasts with the LEO constellation in Figure 42, which creates a very extended cone.

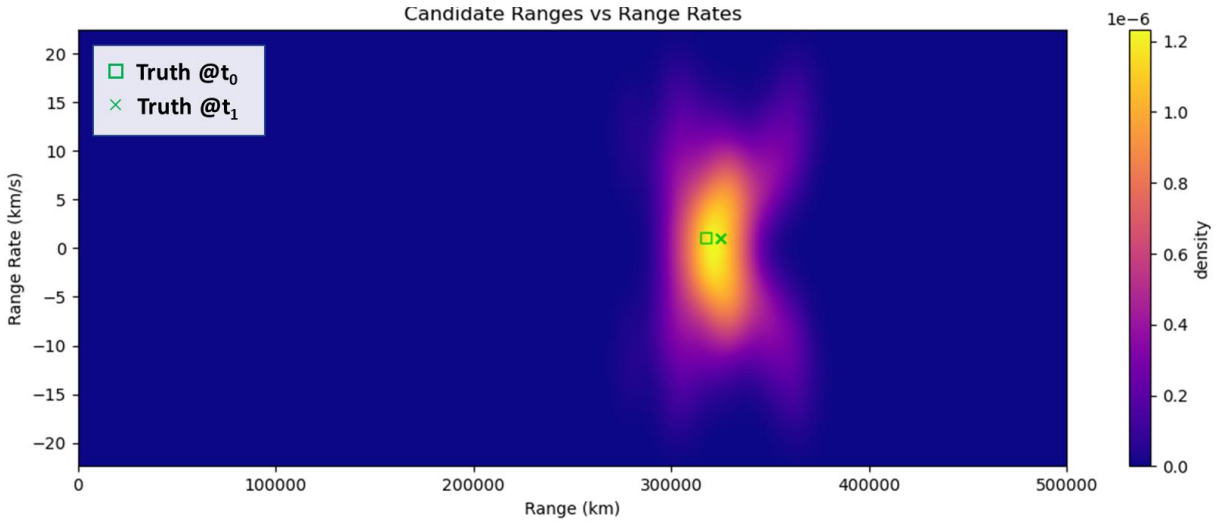

Figure 46: Inclined GEO Constellation Range vs Range Rate Uncertainties

Figure 46 shows a significant decrease in uncertainty vs the LEO constellation for range and range rate. This makes intuitive sense since the range to target has been decreased while increasing measurement diversity, however the range uncertainty is still very significant at tens of thousands of kilometers.

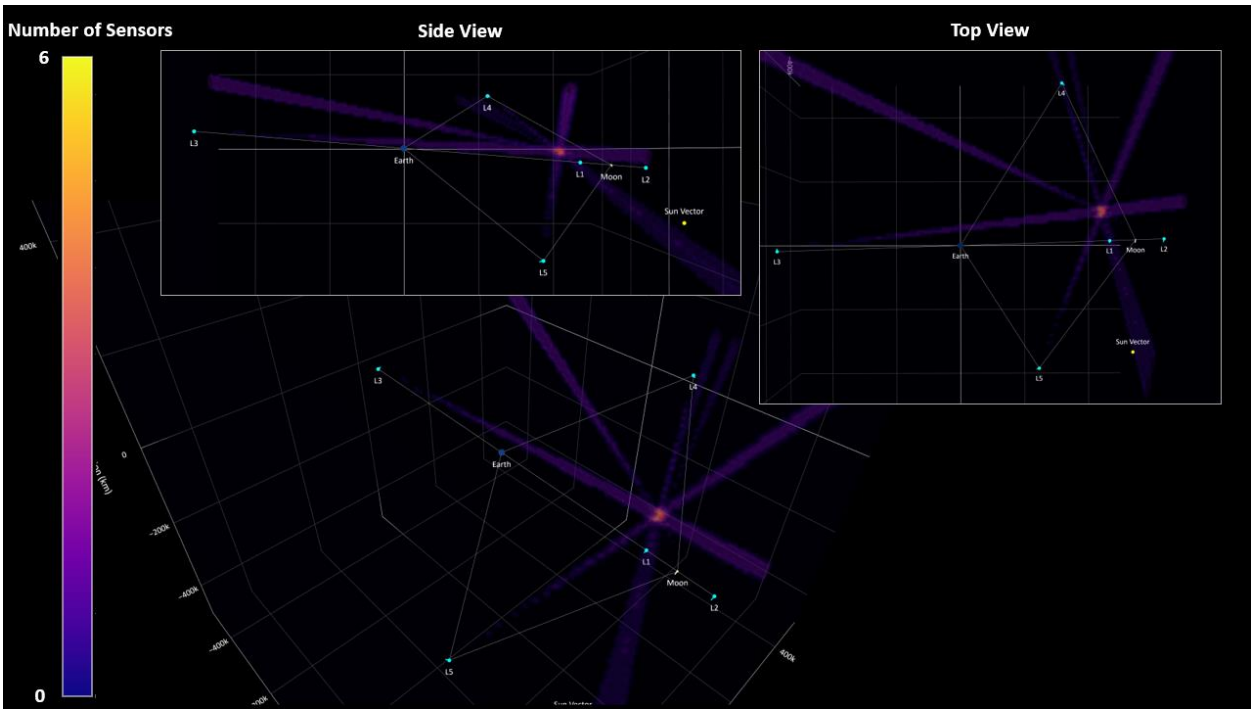

Figure 47: Lagrange Point Constellation Uncertainty Rendering

Figure 47 illustrates an intuitive result for a constellation of Lagrange point observers. With a single observer at each point, we see that the intersections of their FOVs creates a much smaller uncertainty volume.

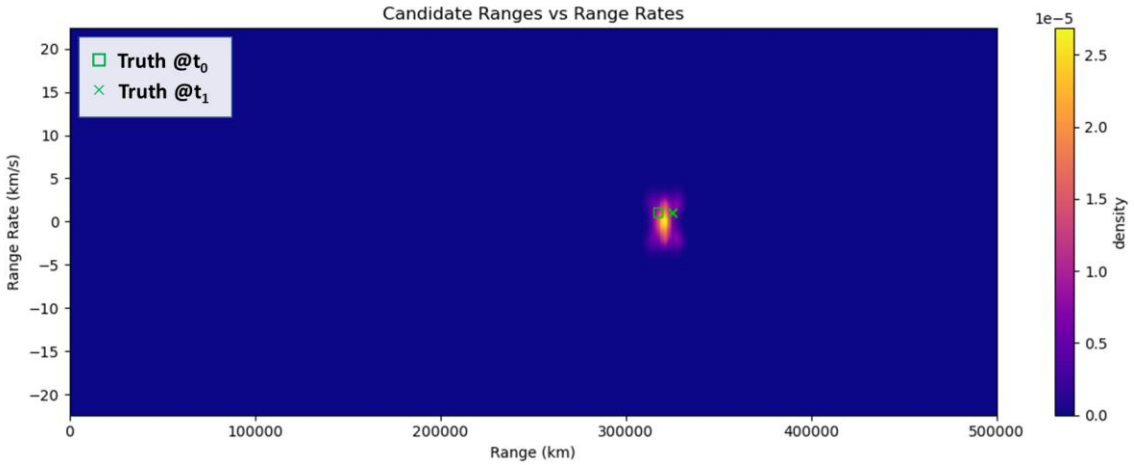

Figure 48: Lagrange Point Constellation Range vs Range Rate Uncertainties

Figure 48 illustrates the significant reduction in uncertainty for range and range rage with this constellation. While this is a compelling result, it is necessary to consider that the analysis in this discussion does not include SNR. The inclusion of SNR will significantly increase the uncertainties. For example, it is highly unlikely that an observer in the L3 orbit would be capable of detecting the object as such a long distance. Furthermore, this does not include any consideration for the stability of the various orbits.

As mentioned previously, additional analysis at much higher resolutions (arcseconds instead of degrees) is necessary to better explore the advantages and disadvantages of different constellations with respect to the TSA challenge. As the resolutions are increased, the performance of all architectures should improve substantially. As these improvements are quantified, the increased accuracy must be balanced with the realism of an architecture and the accuracy necessary to perform the desired objectives.

While higher resolution simulations are necessary to fully understand the cislunar TSA challenge, this analysis is presented to emphasize the importance of considering the impacts of architecture designs on the inherent uncertainties for initial orbit determination from a constellation of observers early in the design phase. While it is possible to construct a constellation of LEO satellites capable of detecting cislunar objects, that does not guarantee that those detections will produce meaningful information content. This is at the core of the Too Short Arc problem. Without a well distributed constellation throughout the cislunar volume it may be possible to detect an object but not possible to determine where it came from or where it might be going within relevant time frames for decision making.

7. CONCLUSIONS

We have reached multiple conclusions based on the modeling/simulation described in this paper. We evaluated potential architectures attempting to perform persistent custody of objects in the cislunar domain with a size of one meter squared and greater. We explored a variety of orbits and concluded that the best foundational orbit type for the architecture needs to provide significant range and solar phase angle diversity to track challenging trajectories. While unstable Lagrange points orbits and chaotic orbits significantly outperform all other identified orbits, they still lack the observation diversity necessary to provide full persistent coverage for more challenging trajectories, such as the free lunar return trajectory during waxing crescent of the Moon. This scenario is representative of multiple scenarios that present significant challenges due to solar phase angle for all constellations in certain conditions. As detailed in this paper, we have concluded a multi-orbit type constellation will most likely be necessary for maintaining persistent coverage of more challenging trajectories leveraging optical sensors with aperture sizes 40cm or less.

Most importantly, performing domain awareness in the cislunar domain poses some very significant challenges when compared to Earth orbiting domains. While these challenges are not “new,” they are very exaggerated in the cislunar domain when compared to LEO or GEO tracking from terrestrial or Earth orbiting domains. These significant challenges require that architecture designs consider and model low Signal-to-Noise Ratios (SNRs), Too-

Short-Arcs (TSAs), and Observing Constellation Orbit Stability (OCOS) as well as other significant challenges such as onboard GNC for observer location knowledge, long range communications, and excessive star clutter which are not covered in this paper.

8. References

[1] B. Weeden and V. Samson, "Op-ed | India's ASAT test is wake-up call for norms of behavior in space," SpaceNews, 8 April 2019. [Online]. Available: https://spacenews.com/op-ed-indias-asat-test-is-wake-up-call-for-norms-of-behavior-in-space/. [Accessed 4 August 2020].

[2] S. Erwin, "Pompeo blasts Iran's space program in wake of military satellite launch," SpaceNews, 26 April 2020. [Online]. Available: https://spacenews.com/pompeo-blasts-irans-space-program-in-wake-of-military-satellite-launch/. [Accessed 4 August 2020].

[3] M. Listner, "Op-ed | A U.S. return to the moon is about preserving the rule of law," SpaceNews, 17 April 2020. [Online]. Available: https://spacenews.com/op-ed-a-u-s-return-to-the-moon-is-about-preserving-the-rule-of-law/. [Accessed 4 August 2020].

[4] J. Foust, "NASA signs agreement with Japan on lunar exploration," SpaceNews, 13 July 2020. [Online]. Available: https://spacenews.com/nasa-signs-agreement-with-japan-on-lunar-exploration/. [Accessed 4 August 2020].

[5] M. Bartels, "Russia wants to land 3 next-generation Luna spacecraft on the moon by 2025," Space.com, 7 May 2020. [Online]. Available: https://www.space.com/luna-russian-moon-lander-program-2020s.html. [Accessed 4 August 2020].

[6] A. Jones, "From a farside first to cislunar dominance? China appears to want to establish 'space economic zone' worth trillions," 15 February 2020. [Online]. Available: https://spacenews.com/from-a-farside-first-to-cislunar-dominance-china-appears-to-want-to-establish-space-economic-zone-worth-trillions/. [Accessed 4 August 2020].

[7] A. Jones, "Chang'e-4 relay satellite enters halo orbit around Earth-Moon L2, microsatellite in lunar orbit," SpaceNews, 14 June 2018. [Online]. Available: https://spacenews.com/change-4-relay-satellite-enters-halo-orbit-around-earth-moon-l2-microsatellite-in-lunar-orbit/. [Accessed 4 August 2020].

[8] D. J. McComas, J. P. Carrico, B. Hautamaki, M. Intelisano, R. Lebois, M. Loucks, L. Policastri, M. Reno, J. Scherrer, N. A. Schwadron, M. Tapley and R. Tyler, "A new class of long-term stable lunar resonanceorbits: Space weather applicationsand the Interstellar Boundary Explorer," *SPACE WEATHER*, vol. 9, no. S11002, pp. 1-9, 2011.

[9] NASA, "NASA - LCROSS Targeting," NASA, [Online]. Available: https://www.nasa.gov/mission_pages/LCROSS/searchforwater/LCROSS_targeting.html. [Accessed 2020 4 August].

[10] J. Carrico, L. Policastri, R. Lebois and M. Loucks, "Covariance Analysis and Operational Results for the Interstellar Boundary Explorer," in *AIAA/AAS Astrodynamics Specialist Conference*, 2010.

[11] C. Scharf, "Crazy, Wonderful, Spacecraft Orbits," Scientific American, 26 May 2015. [Online]. Available: https://blogs.scientificamerican.com/life-unbounded/crazy-wonderful-spacecraft-orbits/. [Accessed 4 August 2020].

[12] NASA JPL, "Animation of PAS-22's trajectory around Earth," HORIZONS System, 6 August 2018. [Online]. Available: https://en.wikipedia.org/wiki/PAS-22#/media/File:Animation_of_PAS-22_trajectory_around_Earth.gif. [Accessed 4 August 2020].

[13] D. J. Dichmann, J. J. Parker, T. W. Williams and C. R. Mendelsohn, "TRAJECTORY DESIGN FOR THE TRANSITING EXOPLANET SURVEY," 2014.

[14] E. Belbruno and J. Carrico, "Calculation of Weak Stability Boundary Ballistic Lunar Transfer Trajectories," in *AIAA/AAS Aatrodynamics Specialist Conference*, Denver, CO, 2000.

[15] NASA, "ARTEMIS - The First Earth-Moon Libration Orbiter," NASA, 13 September 2010. [Online]. Available: https://www.nasa.gov/mission_pages/themis/news/artemis-orbit.html. [Accessed 4 August 2020].

[16] W. F. van Altena, "Signal-to-noise ratio (SNR)," in *Astrometry for Astrophysics: Methods, Models, and Applications*, New York City, NY, Cambridge University Press, 2013, p. 230.

[17] J. Carrico Jr., D. Dichmann, L. Policastri, J. Carrico III, T. Craychee, J. Ferreira, M. Intelisano, R. Lebois, M. Loucks, T. Schrift and R. Sherman, "Lunar-Resonant Trajectory Design for the Interstellar Boundary Explorer (IBEX) Extended Mission," *Advances in the Astronautical Sciences,* vol. 11, no. 454, pp. 771-789, 2012.

[18] A. Milani, G. F. Gronchi, M. D. M. Vitturi and Z. Knezevic, "Orbit determination with very short arcs. I admissible regions.," *Celestial Mechanics and Dynamical Astronomy,* vol. 90, pp. 57-85, 2004.

[19] G. Tommei, A. Milani and A. Rossi, "Orbit determination of space debris: Admissible regions," *Celestial Mechanics and Dynamical Astronomy,* vol. 97, pp. 289-304, 2007.

[20] J. M. Maruskin, D. J. Scheeres and K. Alfriend, "Orbit Determination of Space Debris: Correlation of Optical Observations," in *AMOS,* Maui, 2008.

[21] K. Fujimoto and D. J. Scheeres, "Short-Arc Correlation and Initial Orbit Determination for Space-Based Observations," in *AMOS,* Maui, 2011.

[22] The SciPy community, "SciPy v1.5.2 Reference Guide," SciPy.org, 23 July 2020. [Online]. Available: https://docs.scipy.org/doc/scipy/reference/generated/scipy.stats.gaussian_kde.html. [Accessed 10 August 2020].

[23] K. Ramsley, "Using Lagrange Points to 'stay put'," Brown University, 4 August 2020. [Online]. Available: https://image.slideserve.com/352998/using-lagrange-points-to-stay-put-l.jpg. [Accessed 4 August 2020].